MASSACHUSETTS INSTITUTE OF TECHNOLOGY

LINCOLN LABORATORY

OPTIMUM ELEVATION ANGLE ESTIMATION IN THE PRESENCE OF GROUND REFLECTION MULTIPATH

R. J. McAULAY

Group 44

TECHNICAL NOTE 1976-11

9 FEBRUARY 1976

LEXINGTON MASSACHUSETTS

Abstract

Radars that are developed for the purpose of monitoring aircraft landings in the terminal Air Traffic Control system can be designed to exploit the relatively high signal-to-noise ratio that characterizes the power budgets calculated for such a link. An interferometer using a pair of low gain antennas can be used to obtain passive coverage over a large azimuth and elevation sector. A large base line can be used to obtain the desired elevation angle estimation accuracy. An optimal tradeoff between the width of the subarray aperture and the width of the interferometer base line is performed that achieves a specified elevation angle estimation error while minimizing the overall height of the interferometer configuration. The algorithm searches through the class of antenna patterns that can be synthesized from so-called finite impulse, linear phase digital filters. For the specific problem of designing an elevation sensor for monitoring landing aircraft of final approach, the elevation angle can be estimated with no more than 1-milliradian rms error when the aircraft is within $\pm 60^{\circ}$ azimuth, 2.5° to 40° elevation, using two 7-wavelength subarray antennas spaced 8 wavelengths apart.

In Part II, the design of a separate sensor for resolving the interferometer ambiguities is formulated as a hypothesis testing problem and solved using statistical decision theory. A bound on the probability of an ambiguity error is derived that accounts for the effects of ground reflection multipath and receiver noise. Acceptable performance can be achieved using a 4-element non-uniformly spaced array (0, 3.2, 6.4, 11.2 wavelengths) with relatively inexpensive dipole antennas mounted on tri-plane reflectors.

CONTENTS

LIST OF ILLUSTRATIONS

ILLUSTRATIONS (cont.)

PART II (cont.)

TABLES

PART I

SUBARRAY APERTURE VS INTERFEROMETER BASE LINE

1.0 Introduction and Summary

There are certain practical applications in which direction-finding is to be performed in an environment of high signal-to-noise ratio (SNR). In particular, in the terminal area of the Air Traffic Control (ATC) system, aircraft begin their descent for landing within twenty miles of an airport. Hence, radars developed for the purpose of controlling or monitoring aircraft approaches can exploit the relatively high SNRs that characterize the power budgets calculated for such a link. An interferometer is ideally suited for this situation in view of the fact that a pair of low gain antennas can be used to obtain passive coverage over a large azimuth and elevation sector (i.e., $\pm 60^{\circ}$ azimuth, 0 to 40° elevation), and a large base line can be used to obtain the desired angle estimation accuracy. Furthermore, the antennas and the basic phase measuring equipment can be fabricated to provide reliable low maintenance performance. The ambiguity lobes, which are implicit in the interferometer configuration, can be resolved by utilizing a non-uniformly spaced array in conjunction with minicomputer signal processing. An experimental system referred to as the Precision Altitude and Landing Monitor (PALM) has already demonstrated the efficacy of this technique [Ref. 1].

In Part I of this report, the optimum design of the basic two-element interferometer is presented. In particular, an optimal tradeoff between the width of the subarray aperture and the width of the interferometer base line is performed, with the goal of achieving a specified estimation error while minimizing the overall height of the interferometer configuration. This is accomplished by deriving a sensor design equation that accounts for angle errors as a result of receiver noise, hardware imperfections, and multipath. The errors are expressed in terms of parameters that characterize a large class of antenna patterns (those that can be synthesized for so-called

optimum finite impulse response, linear phase digital filters). By methodically searching through this class of antenna patterns, the optimum interferometer configuration can be determined. For the problem of designing an elevation sensor for monitoring landing aircraft on final approach, it is desirable to estimate the elevation angle with no more than 1-milliradian rms error when the aircraft is within the $\pm 60^{\circ}$ azimuth, 2.5° to 40° elevation coverage region. The optimum solution consists of two 7-wavelength subarray antennas spaced 8 wavelengths apart, which corresponds to an overall width of 15 wavelengths or 13.5 ft at L-band.

The ambiguity resolution issue is considered in detail in Part II of this report. The problem is formulated as a hypothesis testing problem and solved using statistical decision theory. The optimum receiver is a beam forming array that points the antenna beam to each of the ambiguous elevation angles. The true angle is chosen as the one for which the measured power is the largest. An upper bound on the probability of an ambiguity error is derived that accounts for the effects of ground reflection multipath and receiver noise. Numerical results for some obvious designs are given. It is shown that acceptable performance (error rate < 0.004 at worst case phase) can be obtained by using a 4-element nonuniformly spaced array (elements at 0, 3.2, 6.4, 11.2 wavelengths) of relatively inexpensive dipole antennas on tri-plane reflectors.

2.0 Interferometer Design Equations

If a large coverage region is desired using a passive stationary radar, it is necessary to use low gain antennas. As a result of the fact that the directive properties of the antenna pattern are sacrificed in favor of coverage, accurate angle data can be obtained only by measuring the relative phase between two such antennas when they are physically displaced from each other as illustrated in Fig. 1. Such a direction-finding system is referred to as a phase comparison monopulse or an interferometer. When a plane wave of energy is incident upon this radar at an elevation angle e, the phase at the lower antenna lags the phase at the upper antenna by an amount

$$\phi = 2\pi D_B \sin e \tag{1}$$

where D_B is the interferometer base line measured in wavelengths. Let

$$\upsilon = \sin e \tag{2}$$

denote the direction cosine of the incident radiation, then the unknown elevation angle can be estimated from

$$\hat{e} = \sin^{-1} \hat{\upsilon} \tag{3}$$

where

$$\hat{\upsilon} = \phi/2\pi D_B \ . \tag{4}$$

It is immediately apparent that the phase detector can only measure the phase modulo 2π, hence the elevation angle estimate will be ambiguous whenever sin e increases by more than $1/D_B$. It will be shown subsequently that apertures spanning approximately 8 wavelengths will be needed to obtain the requisite accuracy (i.e., $\approx$ 1 milliradian). Due to the fact that coverage up to 40° in elevation is required for terminal area ATC applications, it is apparent that a multiplicity of ambiguity lobes will occur. It is well known

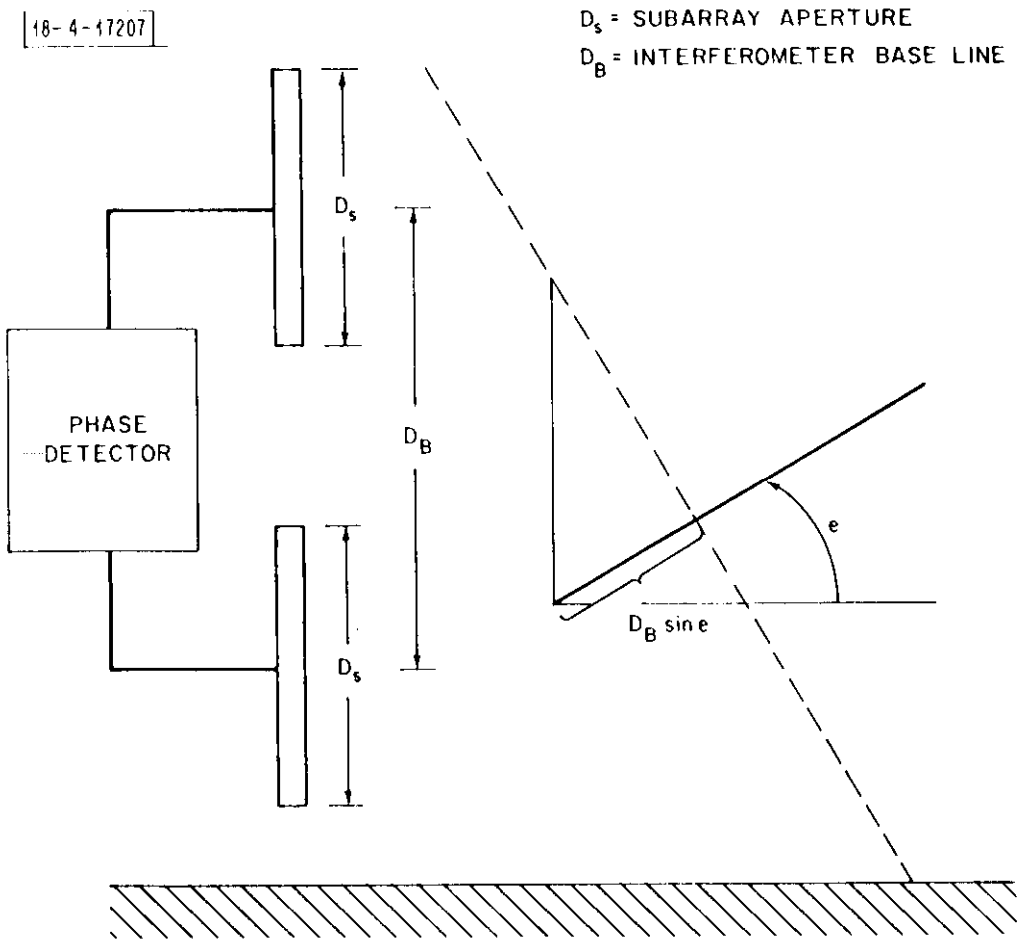

Fig. 1. Phase comparison monopulse or interferometer.

[Ref. 2], however, that the ambiguities can be resolved by the judicious placement of additional antennas to form a sparsely filled array. This is an important issue, which shall be treated separately in Part II of this report. For now, this report will focus on the design of the basic interferometer. In particular an examination has been made of the estimation performance caused by phase measurement errors that arise as a result of the presence of receiver noise, hardware imperfections, and multipath. In the next subsections the basic design equations will be derived that account for phase measurement errors in a quantitative manner that illuminates the hardware design tradeoffs that are possible.

2.1 Front End Noise Error

In practice, the mixer preamplifiers in the front end of each of the channels introduce a noise component, which, through the action of the limiters preceding the phase detectors, results in a noise component being added to the phase term in equation (1). This noise term places a fundamental limit on the accuracy with which the elevation angle can be estimated. Using the Cramer-Rao bounding technique [Ref. 3], it can be shown that this performance limitation for a two-antenna array is given by

$$\sigma_1 = (2\pi D_B)^{-1} \, SNR^{-1/2} \tag{5}$$

where σ_1 refers to the rms error in the estimate of the direction cosine, and SNR denotes the signal-to-noise ratio at the input to the mixer preamplifier. The rms error in the elevation angle estimate is therefore

$$\sigma_e = \sigma_1 / \cos e \tag{6}$$

which, of course, for small e is essentially the same as equation (5). Clearly the estimation error can be made small by either increasing the separation of the antenna pair or increasing the SNR.

For typical applications, the signal-to-noise ratio, in the absence of multipath and antenna pattern considerations, has been conservatively estimated to be 26 dB for an aircraft at 20 mi as indicated in the power budget itemized in Table 2.1. As a basic rule, it was reasonable to work with a 100-watt aircraft transponder that provided an effective radiated power (ERP) of 20 dB relative to 1 watt. For almost all terminal area applications, aircraft will enter the system no farther than 20 miles in range which yields a path loss of -126 dB.

The signal-to-noise ratio will be further increased by the gain of the receiving antenna. However, the actual gain depends on the aperture and amplitude taper of vertical array, which are to be determined by the optimization algorithm. Therefore, at this point the gain must remain unspecified. Regardless of the exact shape of the elevation pattern, however, coverage must extend to within the 3-dB azimuth beamwidth. Therefore, we must anticipate an additional 3-dB loss for an aircraft located at the outer edge of the azimuth coverage region.

In order to eliminate multipath signals caused by buildings, hills, and other aircraft that may be in the coverage region, only 0.2 μsec of the 0.45-μsec pulse is integrated in the receiver. As a result of the fact that the received energy is the power times the time duration, then the factor $10 \log 0.2 \times 10^{-6} = -67$ dB accounts for the associated energy loss. The noise power density, N_0, is -199 dBw/Hz corresponding to a receiver with an effective temperature of 1000°K. The nominal signal-to-noise ratio, SNR_o, is therefore found to be at least 26 dB. Higher accuracy could be achieved by averaging the angle estimates for separate pulses within an ATCRBS reply, e.g., if on the average, eight pulses are present the SNR would be increased by another 9 dB.

TABLE 2.1

POWER BUDGET FOR A TERMINAL AREA ELEVATION BEACON RADAR

Aircraft ERP	20 dBw	100 watts
Path loss	-123 dB	20-mile range
Loss at beam edge	-3 dB	3dB-off boresight
Integration time	-67 dB sec	200 nsec
Noise power density	-199 dBw/Hz	1000° K noise temperature
SNR_o	26 dB	
Gain from averaging over separate pulses of a reply	9 dB	8 pulses present (average)

2.2 Instrumental Errors

Hardware errors manifest themselves as phase measurement errors as a result of the fact that the phase detector characteristics are not perfectly sinusoidal and cannot be completely accounted for using calibration tables. Furthermore, imperfectly cut cable lengths and temporal variations in receiver characteristics also result in drifts that are difficult to completely eliminate. Since

$$\phi = 2\pi D_B \sin e \tag{7}$$

then

$$\sigma_2 = (2\pi D_B)^{-1} \sigma_\phi \tag{8}$$

where σ_2 is the corresponding error in the estimate of the direction cosine, and σ_ϕ is the rms phase measurement error.

2.3 Multipath Errors

The final source of error to be considered is caused by ground multipath. It has been determined in reference [4] that multipath will produce a phase measurement error given by

$$\delta\phi = \tan^{-1}\left(\frac{\rho \sin\theta_1}{1 + \rho \cos\theta_1}\right) - \tan^{-1}\left(\frac{\sin\theta_2}{1 + \rho \cos\theta_2}\right) \qquad (9)$$

where ρ is the ratio of the multipath to direct signal level measured at the output of the antennas, and θ_i is the phase of the multipath relative to the direct signal at the i^{th} antenna. Considering a worst case for θ_1 and θ_2* yields

$$\delta\phi = 2 \sin^{-1} \rho \quad . \qquad (10)$$

As a result of the fact that the previous expressions have been in terms of rms values, introducing the worst case multipath error may result in an overly pessimistic design, especially because the worst case values of θ_i are not $\pm \pi$. If instead we assume that the θ_i are independent random variables uniformly distributed over $(-\pi, \pi)$, it is found that

$$\overline{\delta\phi} = 0$$

$$\overline{\delta\phi^2} \approx \rho^2 \text{ to terms in } \rho^4 \quad . \qquad (11)$$

Using σ_3 to denote the corresponding (rms) error in the elevation angle direction cosine, and applying equation (7), it is seen that†

$$\sigma_3 = (2\pi D_{13})^{-1} \rho \quad . \qquad (12)$$

2.4 Antenna Pattern Effects

The primary discriminant against ground reflection multipath is the antenna pattern developed on the subarray aperture. In order to account for the way in which the antenna design affects the SNR and multipath, this

---

*$\theta_1 = \cos^{-1} \rho$, and $\theta_2 = \pm \cos^{-1} \rho$.

†For small values of ρ, the rms error is half the peak error.

section is concerned with the canonical antenna pattern illustrated in Fig. 2. The pattern is designed for coverage over a region e_{min} to e_{max}. Within this region, the mainlobe has ripples of magnitude $20 \log (1 + \delta_p)/(1 - \delta_p)$ dB, controlled by the parameter δ_p. For a flat earth it is expected that the multipath will arrive within the region $-e_{min}$ to $-e_{max}$. Within this region the sidelobes are $20 \log \delta_s$ less than the nominal antenna gain, being controlled by the parameter δ_s. Due to the fact that the transition region from the passband to the stopband is fixed at $2\, e_{min}$, then the ability to achieve the specified passband and stopband ripples will depend on the width of the subarray aperture that is available on which the pattern is to be synthesized.

As a result of the target and multipath signals impinging on the antenna beam at angles above e_{min} and below $-e_{min}$, respectively, the effective reflection coefficient measured at the antenna output is always less than

$$\rho_{eff} \leq \frac{\delta_s}{1 - \delta_p}\, \rho(e), \qquad e \geq e_{min} \tag{13}$$

where $\rho(e)$ is the reflection coefficient measured at the antenna input for targets at elevation angle e. Therefore from equation (11), the rms error in the elevation angle estimate caused by multipath is always less than

$$\sigma_3 = (2\pi D_B)^{-1}\, \frac{\delta_s}{1 - \delta_p}\, \rho(e) \quad . \tag{14}$$

Intuitively, it is suspected that the larger the subarray aperture, the smaller will be the ratio of stopband ripple to lower edge passband attenuation, $\delta_s/(1 - \delta_p)$, thus reducing the multipath induced error. With the realization that smaller errors are also achieved by increasing the interferometer base line, equation (14) begins to illustrate the tradeoff that exists between the width of the subarray aperture and the interferometer base line.

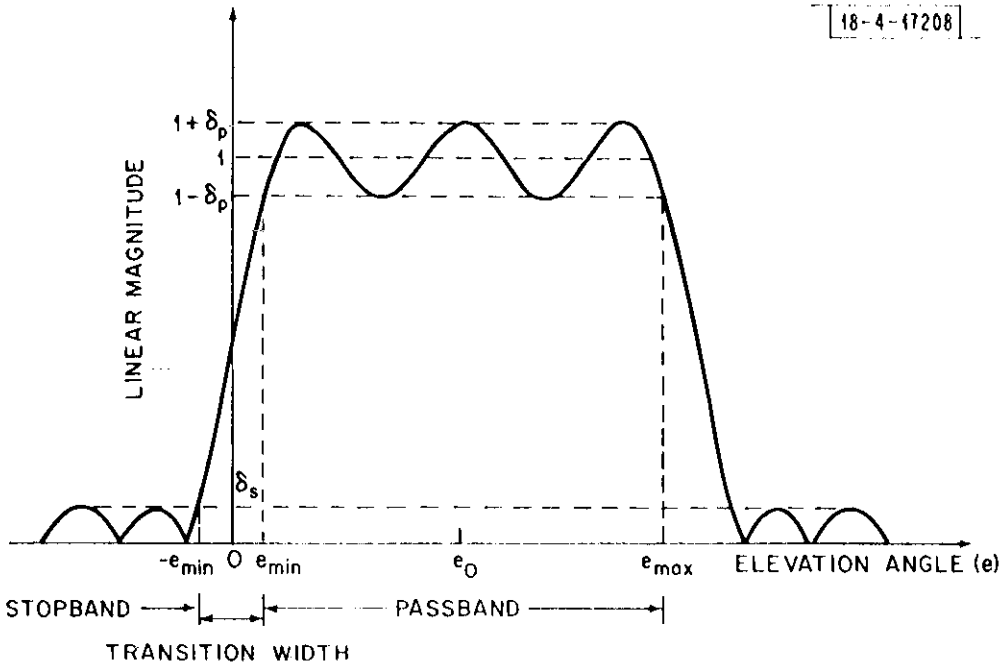

Fig. 2. The canonical antenna pattern.

In addition to reducing the multipath induced angle errors, the shaped beam developed on the subarray aperture also has some gain that may enhance the signal-to-noise ratio of the link and thus improve performance. Due to the fact that worst-case performance is being designed, care must be taken to account for power losses as a result of the target signal impinging on the antenna at the passband edge. First, the gain is calculated for an antenna using a uniform illumination to obtain coverage over an elevation sector of width $BW_{e\ell}$, and an azimuth sector of width BW_{az}. The gain is simply

$$G_o = 4\pi \left(\frac{50.9}{BW_{az}}\right) \left(\frac{50.9}{BW_{e\ell}}\right) \quad . \tag{15}$$

In practice, the antenna is to be fabricated using radiating dipoles with half-wavelength spacing over a ground plane. The width of the ground plane is chosen to have a 3-dB azimuth beamwidth of BW_{az}. In other words, no amplitude tapering is being developed for the azimuth beam, and the contribution to the gain equation will be given by the second term in equation (15). In the elevation plane, however, significant amplitude tapering will be used in order to obtain the sector beam with the sharp lower edge cutoff. If N elements are to be used in the vertical array (with half-wavelength spacing), the width of the aperture is (N - 1)/2. For a uniformly illuminated array, the beamwidth would be

$$BW_{e\ell} = 50.9\left(\frac{2}{N - 1}\right) \tag{16}$$

and the gain in equation (15) would be

$$G_o = 2\pi\ (N - 1)\left(\frac{50.9}{BW_{az}}\right) \quad . \tag{17}$$

For an array in which the half-wavelength excitations are tapered according to the coefficients

$$\{a_n\}_{n=0}^{N-1}$$

the antenna pattern is

$$A(e) = \sum_{n=0}^{N-1} a_n \exp(i n\pi \sin e) \quad . \tag{18}$$

The gain of this pattern is the gain for the uniform illumination reduced by a factor referred to as the taper efficiency [Ref. 5] and is given by

$$\eta = \frac{(\Sigma a_n)^2}{N \Sigma a_n^2} \quad .$$

Hence, the gain in the boresight direction is

$$G_o = 2\pi\eta (N - 1) \left(\frac{50.9}{BW_{az}}\right) \tag{20}$$

and is, therefore, a function of the antenna pattern generated by the synthesis procedure. The SNR calculated in the power budget analysis in Table 2.1 is therefore increased to

$$SNR (N;\underline{a}) = G_o (N;a) \cdot SNR_o \tag{21}$$

where the notation SNR(N;a) is used as a reminder of the dependence on the width of the subarray aperture and the elevation taper coefficients $a_1\ a_2 \cdots a_N$.

Additional losses in signal power will occur as a result of attenuation by the passband edge and multipath fading. At the output of the antenna the amplitude of the target signal, which has incident amplitude A_s and is located in the center of the passband, will be $A_S\sqrt{G_o}$. From equation (18), the amplitude of the antenna pattern on boresight is Σa_n, whereas its value at the

passband edge is $1 - \delta_p$. Therefore, if the target is located at the passband edge, its amplitude will be reduced to

$$A_S' = A_S \sqrt{G_o} \frac{1 - \delta_p}{\Sigma a_n} \quad . \tag{22}$$

Similarly the amplitude of the multipath signal at the stopband edge will be

$$A_I' = \rho(e_{min})\, A_S \sqrt{G_o} \frac{\delta_s}{\Sigma a_n} \quad . \tag{23}$$

Due to the fact that this can combine out of phase with the direct signal, multipath fading can occur, which reduces the signal amplitude to

$$A_S' - A_I' = A_S \sqrt{G_o} \frac{1 - \delta_p - \rho(e_{min})\, \delta_s}{\Sigma a_n} \quad . \tag{24}$$

Therefore, the reduction in amplitude relative to the boresight value is simply $[1 - \delta_p - \rho(e_{min})\, \delta_s]/\Sigma a_n$. Thus, the increase in SNR, as a result of antenna gain, is offset by losses caused by passband cutoff and multipath fading, which results in an effective operating signal-to-noise ratio of

$$SNR(N;\underline{a}) = SNR_o + 20 \log \left[2\pi\eta\,(N - 1)\left(\frac{50.9}{BW_{az}}\right)\right] + 20 \log \left[\frac{1 - \delta_p - \delta_s\, \rho(e_{min})}{\Sigma a_n}\right] \tag{25}$$

where SNR_o refers to the 26-dB value computed in Table 2.1. It should be noted that all of the quantities are easily computed at each step of the iterative process. The above SNR value is used to include the effects of these losses in the elevation angle error caused by the receiver noise. The contribution to the rms angle error, equation (5), becomes

$$\sigma_1 = (2\pi D_B)^{-1}\, SNR(N;\underline{a})^{-1/2} \quad . \tag{26}$$

2.5 Sensor Design Equation

Due to the fact that errors caused by noise, hardware imperfections and multipath are independent, they can be added in an rms sense to give the total error design equation. Therefore, combining equations (8), (14) and (26), this equation becomes

$$\sigma_{\text{sine e}} = (\sigma_1^2 + \sigma_2^2 + \sigma_3^2)^{1/2}$$

$$= (2\pi D_B)^{-1} \left\{ \frac{1}{SNR(N; \underline{a})} + \sigma_\phi^2 + \left[\frac{\delta_s}{1 - \delta_p} \cdot \rho(e_{min}) \right]^2 \right\}^{1/2} \quad (27)$$

For a given subarray aperture (which fixes the number of elements N) and a given aperture taper, δ_p and δ_s can be determined, and the values for equation (25) and the bracket term in equation (27) can be computed. The interferometer base line can then be chosen to yield the desired accuracy σ_D milliradians. For tactical military operations, it is essential that the overall height of the array be as small as possible. Therefore, it is desired to find that aperture taper (and corresponding subarray aperture width D_S^*) and interferometer base line D_B^* such that the σ_D milliradian accuracy is achieved and $D_B^* + D_S^*$, the total width of the interferometer, is a minimum. In order to solve this optimization problem it will first be necessary to establish an antenna pattern synthesis technique that exhausts the class of antenna patterns having the canonical antenna pattern illustrated in Fig. 2 for which the sensor design equation was derived; this is the topic to be discussed in Section 3.0.

3.0 Optimum Antenna Pattern Synthesis

In order to design an antenna pattern that satisfies the constraints on coverage and ripple widths illustrated in Fig. 2, information contained in the paper by Evans [Ref. 6] and analogous work in the area of digital filter design will be used. In particular, the results of Parks and McClellan [Ref. 7], which is a filter synthesis method that minimizes the approximation error to an ideal bandpass filter, shall be used. The optimization is performed over the class of finite impulse response (FIR), linear phase digital filters. The mapping from elevation angle space, e, to frequency space F is defined by the relation

$$F = 0.5\ (\sin e - \sin e_o) \quad . \tag{28}$$

The solution to the filter design problem yields a frequency characteristic that is symmetrical about DC; whereas in the antenna design case, the pattern is to be located in such a way that the center of the transition region is located on the horizon. This translation is accounted for by the $\sin e_o$ term in equation (28) from which e_o can be intepreted as the electrical tilt angle and can be implemented by applying an appropriate phase taper to the antenna elements.

In the antenna design problem, the maximum and minimum elevation angles (e_{max} and e_{min}) over which passband coverage is to be obtained are specified. These elevation angles correspond to the passband and stopband edges F_p and F_s in the filter design problem. The duality is more clearly demonstrated by comparing the filter design specifications indicated in Fig. 3 with those for the antenna illustrated in Fig. 3. From this comparison, the following relations can be written:

$$F_p = 0.5[\sin e_{max} - \sin e_o] \tag{29a}$$

$$-F_p = 0.5[\sin e_{min} - \sin e_o] \tag{29b}$$

$$-F_s = 0.5[\sin(-e_{min}) - \sin e_o] \quad . \tag{29c}$$

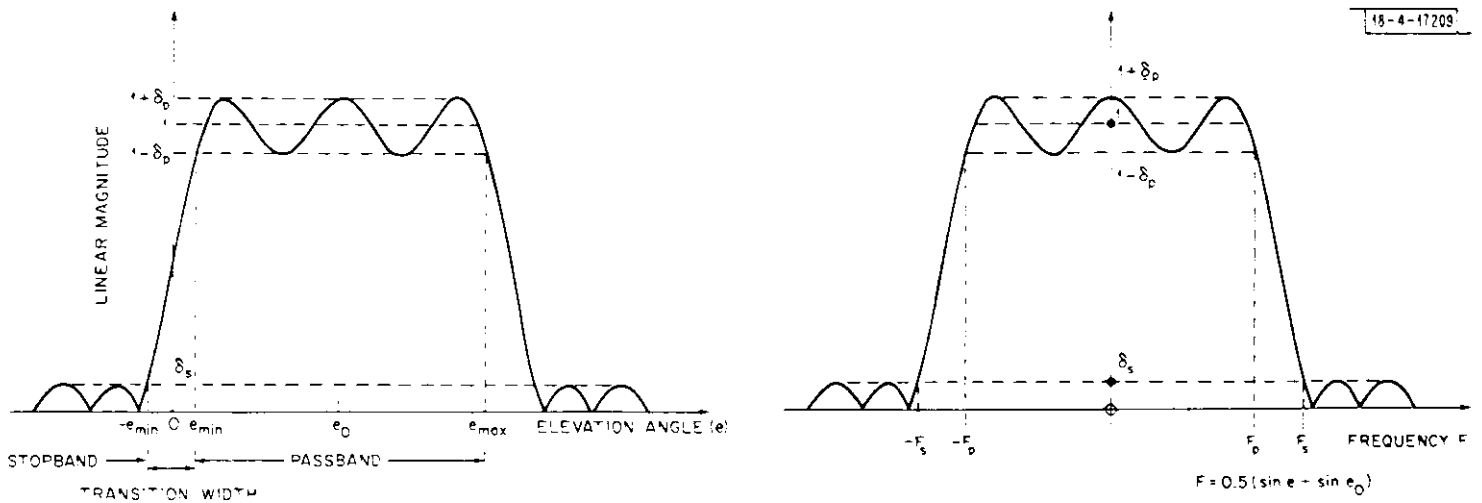

Fig. 3. Filter design, antenna design duality.

From these equations, it is found that

$$F_p = 0.25[\sin e_{max} - \sin e_{min}] \tag{30a}$$

$$F_s = F_p + \sin e_{min} \tag{30b}$$

$$e_o = \sin^{-1}\left(\frac{F_p + F_s}{2}\right) \quad . \tag{30c}$$

The optimum FIR digital filter synthesis algorithm also requires specification of the number of filter coefficients, N, and the ratio

$$K = \delta_p/\delta_s \quad . \tag{31}$$

The algorithm then generates the finite impulse response that minimizes (in a minimax sense) the approximation error to an ideal low pass filter and results in the corresponding values of δ_p and δ_s. The computer program used was (with minor modifications) the same as that described and documented in [Ref. 8]. The design algorithm is implemented by specifying K and F_p and F_s, which fix the transition width; then the deviation δ_s and also $\delta_p = K\,\delta_s$ are minimized. Figure 4 illustrates some of the experimental results of the relationships between these parameters obtained by Parks and McClellan [Ref. 7]. Figure 4(a) plots δ_p vs F_p for a length 29 filter, which indicates that a 3.32-dB fluctuation in the sidelobe level can be obtained by varying the location of the passband edge. This rather peculiar behavior has significant implications regarding the synthesis of antenna patterns and will be presented in Section 4.0. Figure 4(b) indicates the reduction in sidelobe level that is possible by increasing the length of the filter. In terms of the antenna pattern design, this simply indicates that larger apertures can achieve lower sidelobe levels, which in turn means a reduction in the effects of multipath.

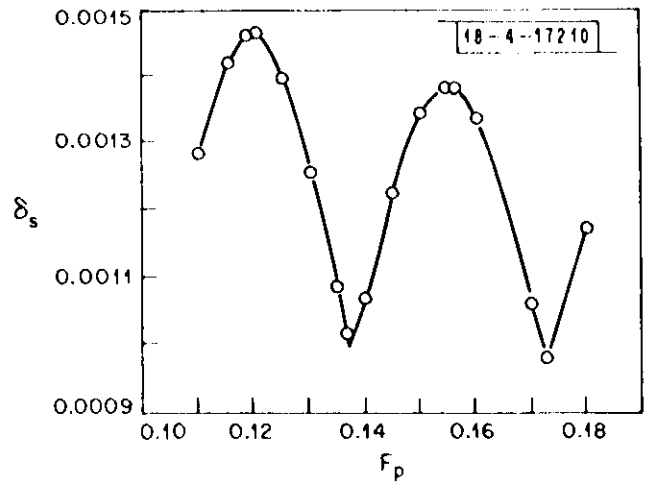

Fig. 4(a). Influence of passband edge F_p on stopband deviation δ_s for fixed transition width TW = 0.09 and weighting factor K = 10 with length 29 filter.

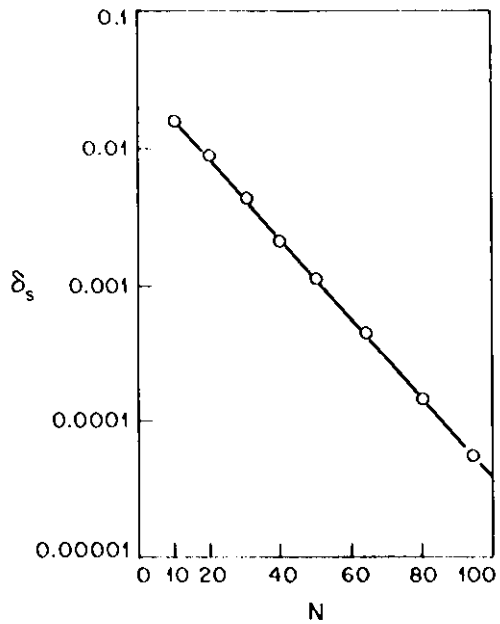

Fig. 4(b). Dependence of stopband deviation δ_s on filter length for passband edge F_p = 0.2, stopband edge F_s = 0.24 and weighting factor K = 50.

In Section 4. 0 this filter design algorithm will be applied to generate a large class of optimum antenna patterns. The parameters of the antenna patterns are used to evaluate the sensor design equations developed in the preceding section. This aids in the performance of the tradeoff between the subarray aperture and the interferometer base line.

4.0 Optimum Interferometer Design

The results of the preceding sections shall now be combined to develop a methodology for performing an optimum tradeoff between the interferometer base line and the subarray aperture. To begin, the number of elements in the array are fixed at N. This fixes the width of the subarray aperture at

$$D_S = (N - 1)/2 \tag{32}$$

where one-half-wavelength separation between elements has been assumed. For this value of N, a value for the parameter $K = \delta_p/\delta_s$ is then chosen, and the corresponding optimum antenna pattern is designed, which results in optimal values of δ_p and δ_s. These values are applied to the sensor design equation, equation (30), and solved for the interferometer base line needed to yield a σ_D milliradian estimation error for a target at the minimum elevation angle, e_{min}. Solving equation (30) for D_B gives

$$D_B(K;N) = \left(\frac{1000}{2\pi\sigma_D}\right)\left\{\frac{1}{SNR(N;\underline{a})} + \sigma_\phi^2 + \left[\frac{\delta_s}{1 - \delta_p}\,\rho(e_{min})\right]^2\right\}^{1/2} . \tag{33}$$

As a consequence, for fixed N, different values of K result in different optimal antenna tapers with different values of δ_p, δ_s and boresight gain; hence the interferometer base line needed to ensure the σ_D milliradian error is indeed functionally dependent on the weighting parameter K. Therefore, a search is performed over all possible values of K to determine the minimum interferometer base line $D_B^*(N)$. The total aperture width of the interferometer is then

$$D_T(N) = (N - 1)/2 + D_B^*(N) \tag{34}$$

which depends on only the number of antenna elements N. A search is then performed over integer values of N until the aperture of the antenna complex is minimized.

The foregoing ideas can be demonstrated most clearly by way of an example: Suppose it is decided to design an interferometer for monitoring aircraft landings in which the rms errors are to be no larger than 1 milliradian. Coverage from 2.5° to 40° in elevation is required over an azimuth sector $\pm 60^{\circ}$ in extent. For multipath reflections from flat dry gound, the magnitude of the reflection coefficient as a function of aircraft elevation angle is illustrated in Fig. 5. For an aircraft at the minimum elevation angle, 2.5°, the reflection coefficient is -3 dB. Assuming that it is possible to construct a receiver in which the phase measurement errors caused by hardware imperfections will be less than 1.5 electrical degrees, the following set of parameter values are established:

$$SNR_o = 26 \text{ dB}$$

$$\sigma_D = 1 \text{ milliradian}$$

$$e_{max} = 40^{\circ}$$

$$e_{min} = 2.5^{\circ}$$

$$\rho(e_{min}) = -3 \text{ dB}$$

$$\sigma_\phi = 1.5^{\circ} \text{ (electrical)} \quad .$$

The passband and stopband cutoff frequencies are then determined and used as an input to the filter design program. In the next step, the number of elements in the subarray is fixed, e.g., N = 10, which gives a subarray aperture of 4.5 wavelengths. If a uniform illumination were applied to the aperture, the antenna gain would be 13.9 dB. In fact, the filter synthesis algorithm results in nonuniform distributions that are functionally dependent on the parameter $K = \delta_p/\delta_s$, e.g., with K = 10.0, the loss in gain caused by the use of a tapered amplitude distribution, as measured by the taper efficiency, equation (19), is -2.3 dB. In addition the synthesis program outputs

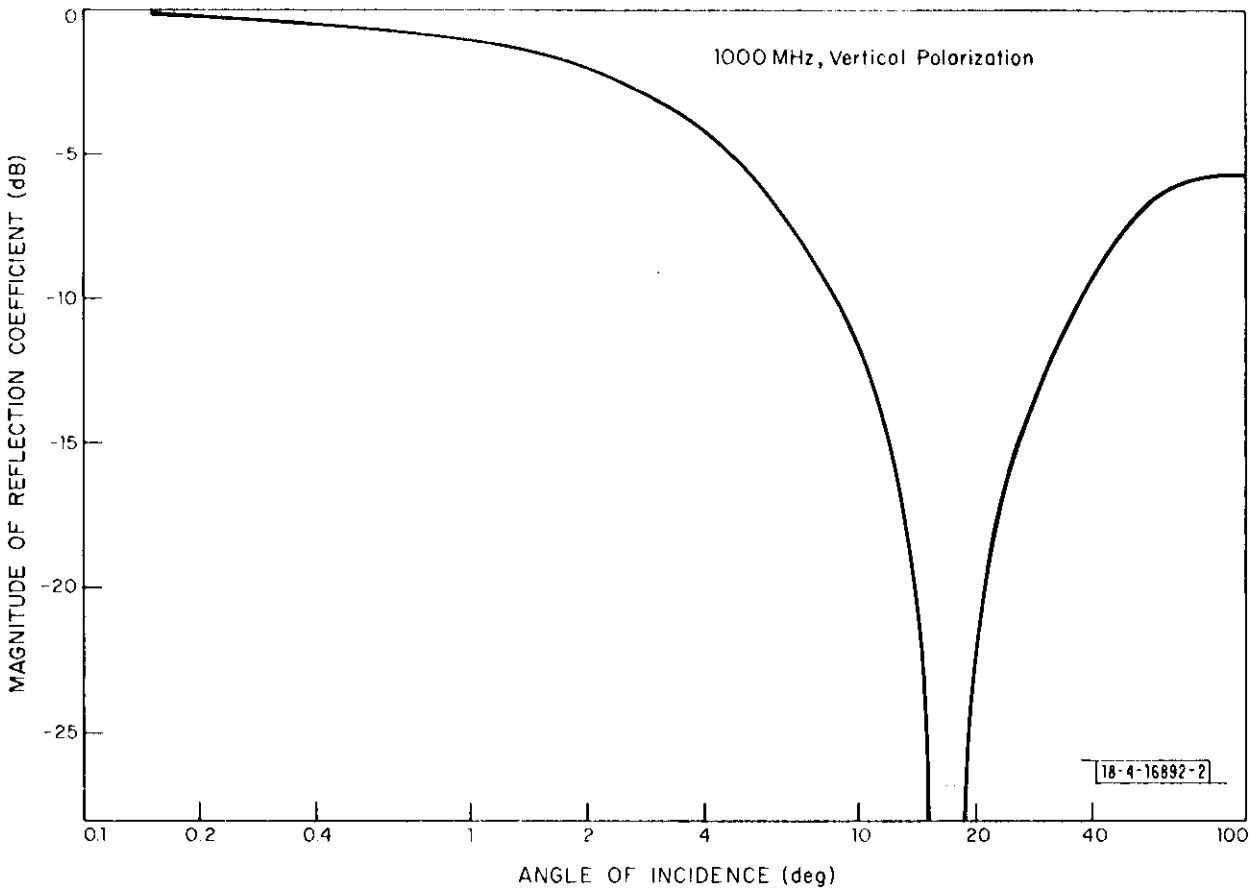

Fig. 5. Reflection coefficient for smooth, flat, dry land vs angle of incidence.

the minimizing values of δ_p and δ_s. In this case the values are $\delta_p = 0.5947$, and $\delta_s = 0.05947$ corresponding to 11.9-dB passband ripples and -28.6-dB sidelobes relative to the boresight gain. The numerical values of δ_p and δ_s are then used in the sensor design equations (25) and (27) to determine the effects of the passband attenuation and multipath, e.g., at 2.5° elevation, the target signal will be attenuated an additional -11.9 dB as a result of the lower edge cutoff of the antenna pattern. When the effect of a fade caused by multipath is considered, the loss increases to -14.47 dB. These losses, as well as the effects of the multipath induced angle errors, are accounted for simply by substituting their values for the effective gain and passband and sidelobe levels into equations (25) and (27), which then yields the interferometer base line that is needed to support 1-milliradian-rms angle error. For the preceding values, the required base line is 20.4 wavelengths. Combined with the 4.5-wavelength width of the subarray aperture, the total interferometer width (when K = 10.0) is 24.9 wavelengths. Of course, varying K will cause this total width to vary, and in order to find the smallest possible width a search over a range of values of K is required. The results for the 10-element subarray are plotted in Fig. 6. The minimum interferometer aperture in this case is 23.75 wavelengths at K = 26.5 ($\delta_p = 0.7151$, $\delta_s = 0.0269$).

It should be emphasized that the preceding design for a 10-element array is the optimum, dependent upon the condition that the upper edge of the passband is required to be precisely 40° ($e_{max} = 40^\circ \rightarrow F_p = 0.321$). However, in Section 3.0, it was indicated that the optimum filter designs were functionally dependent on the passband cutoff frequency, $F_p[0.5(\sin e_{max} - \sin e_o)]$. In the antenna design problem, there is some flexibility in the actual coverage region specification, and it is therefore important to explore the sensitivity of the optima with respect to the parameter e_{max}. This is plotted in Fig. 7, which illustrates the minimum interferometer aperture as a function of the maximum elevation angle for which specified coverage is desired, viz e_{max}. For a fixed number of elements, it is apparent that the fluctuation in the minimum aperture width can be significant. For the 10-element design, the aperture for a 40° coverage is 23.75

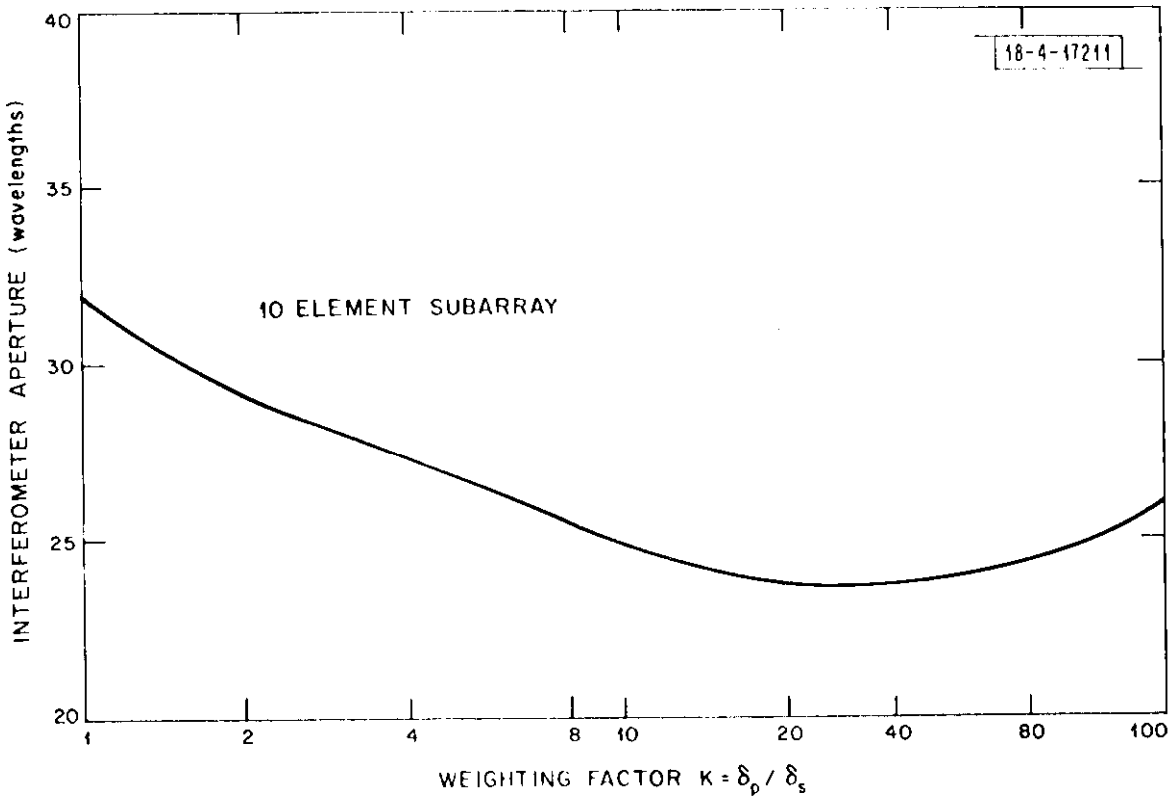

Fig. 6. Optimum interferometer width vs K (= δ_p/δ_s).

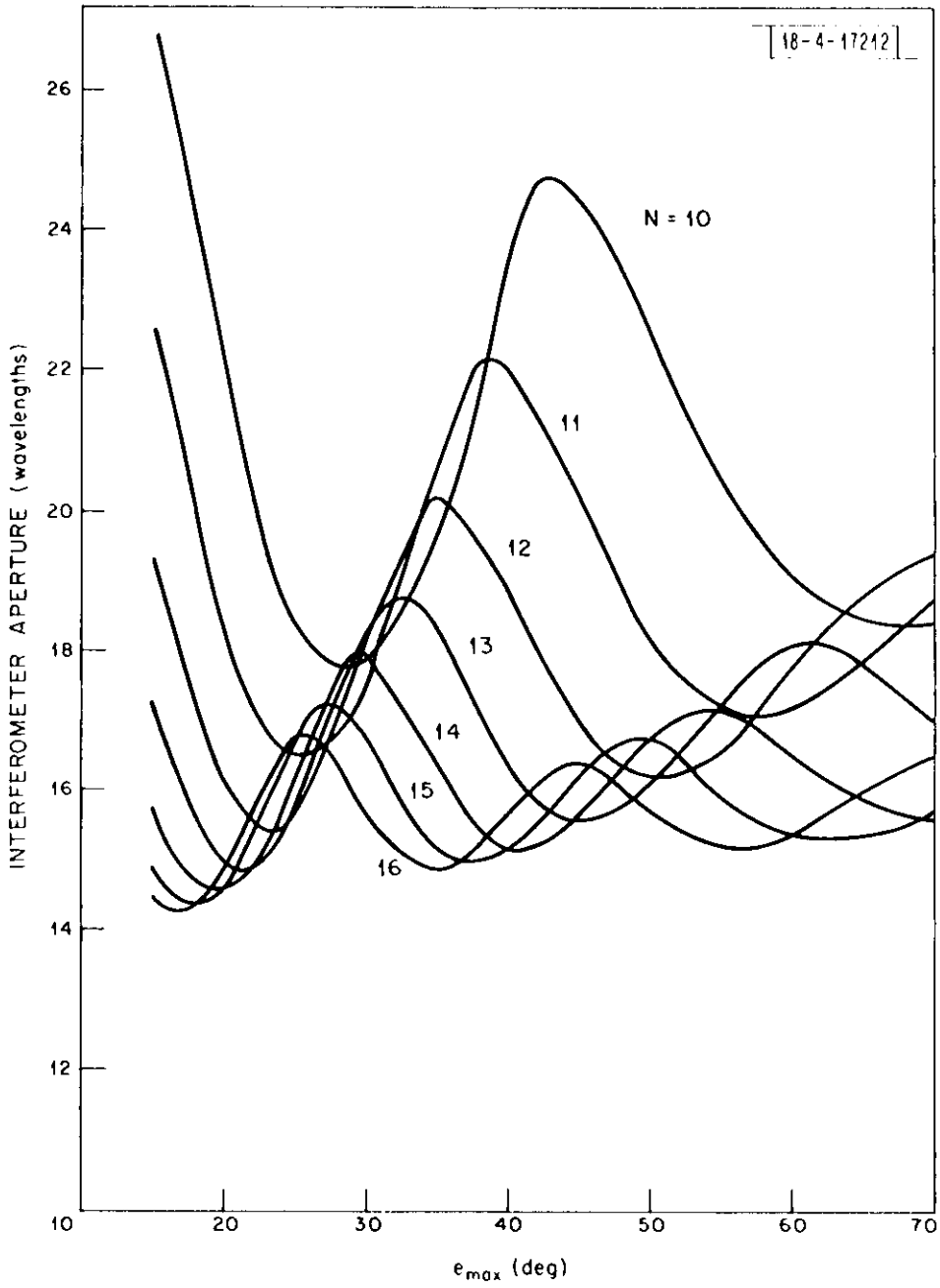

Fig. 7. Optimum interferometer width vs e_{max}.

wavelengths, but only 18.4 wavelengths if the coverage region is expanded to 66°. Due to the fact that there is no loss in using an antenna pattern that gives larger coverage, it is obvious that the latter design should be used. Also plotted were the minimum aperture widths for 11-through 15-element designs versus the coverage parameter e_{max}. In each case the best design operating point is chosen to be the value of e_{max} no smaller than 40° for which the overall aperture is a minimum. The results are tabulated in Table 4.1. Also tabulated was the slope of the antenna pattern at the horizon, and the parameter $K = \delta_p/\delta_s$ because these give an indication of the likely sensitivity of the performance to antenna hardware errors.

TABLE 4.1

CHARACTERISTICS OF OPTIMIZED DESIGNS

Number of Elements	Interferometer Aperture (wavelengths)	Maximum Elevation Angle (degrees)	Horizon Slope (dB/deg)	$K = \delta_p/\delta_s$
10	18.4	67.5	3.67	13.66
11	17.1	58.0	3.79	15.78
12	16.2	50.5	3.84	15.85
13	15.6	45.5	4.22	17.30
14	15.2	41.0	4.23	14.74
15	15.0	37.0	4.29	17.05
16	14.9	35.0	4.57	19.90

Although the design for a 16-element array would probably be acceptable from a coverage point of view, it cannot be used in practice because the interferometer base line is 7.4 wavelengths, which is smaller than the physical separation required for the two 7.5-wavelength apertures of the subarrays. The smaller base line could only be accommodated by offsetting the azimuth boresight axis of the two subarrays which would then cause an additional phase shift to the interferometer measurement whenever the aircraft was not in the azimuth boresight plane. Therefore, the optimal solution is obtained by the 15-element subarrays (7 wavelengths wide) spaced 8 wavelengths apart. It is interesting that the optimum solution is essentially a filled aperture.

The optimum antenna pattern is illustrated in Figs. 8, 9, and 10. The amplitude taper needed to generate the optimum antenna pattern is illustrated in Fig. 11. A linear phase taper would also be applied to the elements in order to electrically steer the beam to center the pattern at 19.0° in elevation. If a uniform taper were applied to the same physical aperture, the antenna gain would be 15.8 dB. However, the taper used to obtain the sharp cutoff and sector beam coverage has a taper efficiency of -11.5 dB. The signal loss as a result of the attenuation at the passband edge is 0 dB indicating that the boresight gain occurs on the boundary of the passband constraint region ($1 \pm \delta_p$). When the possibility of a multipath fade is considered, another -0.4 dB loss is incurred. Adding all of these effects produces an effective output SNR of 29.8 dB, which is the number used in calculating the contribution to the rms error caused by receiver noise. It was found that the sidelobes were -27.9 dB down from the boresight gain; and because the boresight gain and the gain at the passband edge are equal in this particular case, the multipath is -30.9 dB lower than the direct signal (a -3 dB-multipath reflection coefficient was assumed). The final parameter of interest is the slope of the antenna pattern at the horizon which indicates how fast the lower edge cutoff is rolling off. For this example, it proved to be 4.3 dB/deg, which may not be unreasonable to maintain in practice. In case it is unreasonable and other designs must be chosen for practical reasons, the horizon slope and the interferometer widths for the optimum designs (as a function of N) have been tabulated in Table 4.1.

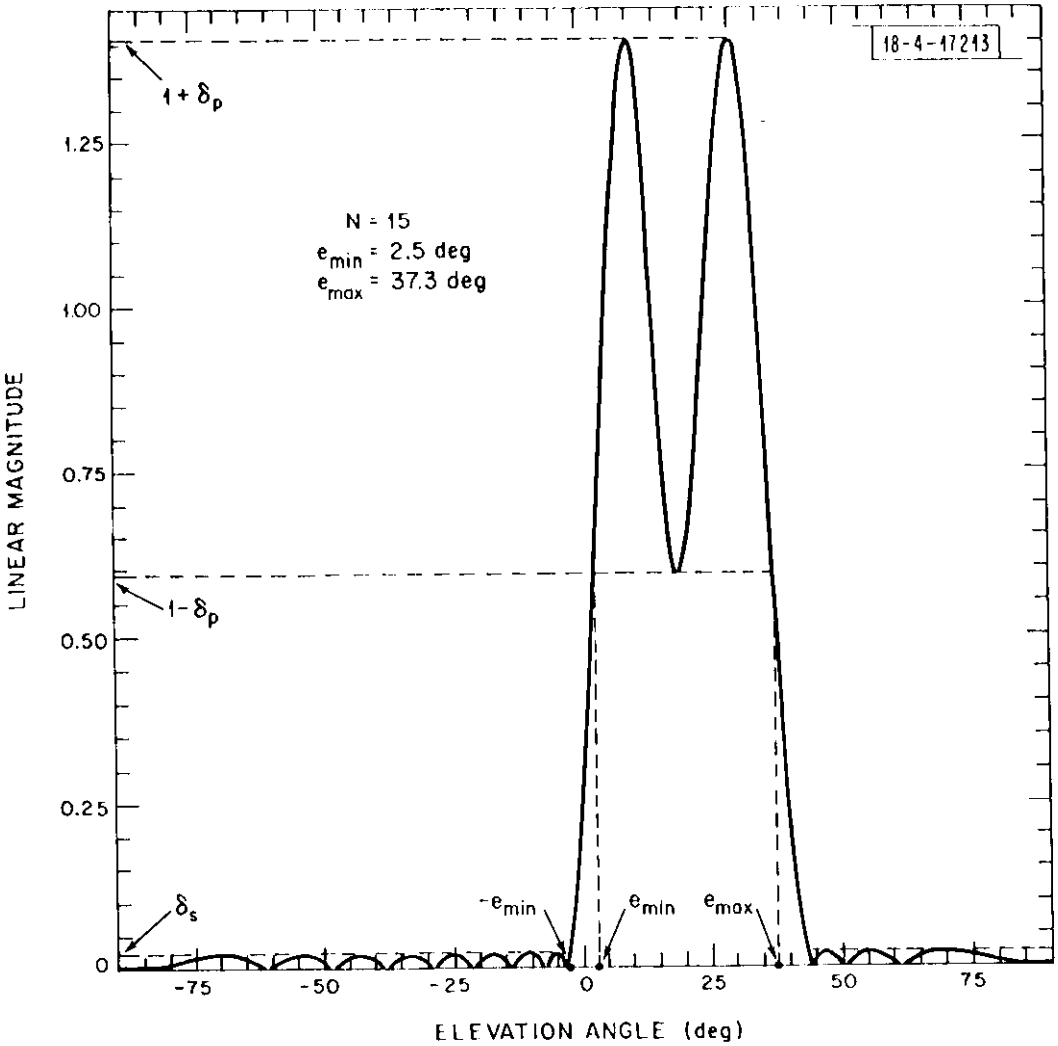

Fig. 8. Subarray antenna pattern (linear scale).

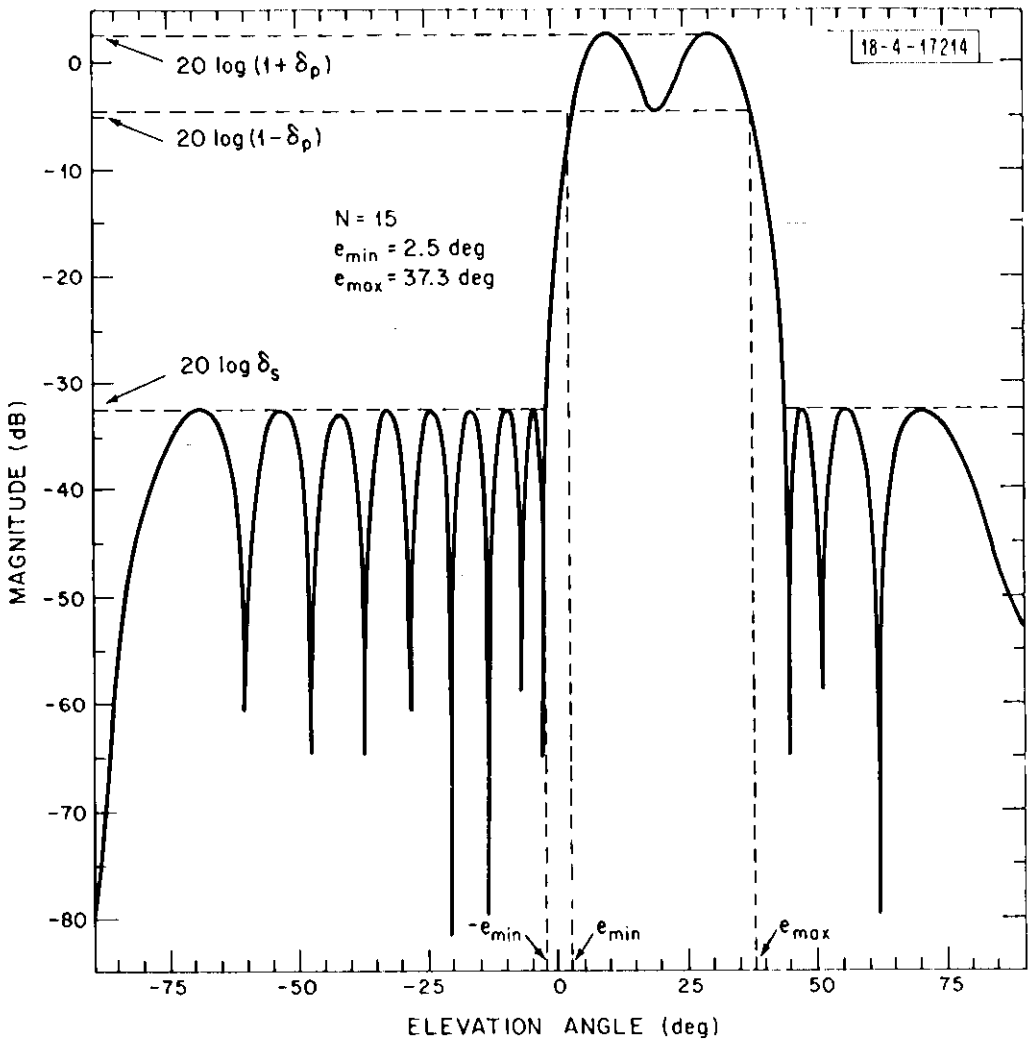

Fig. 9. Subarray antenna pattern (logarithmic scale).

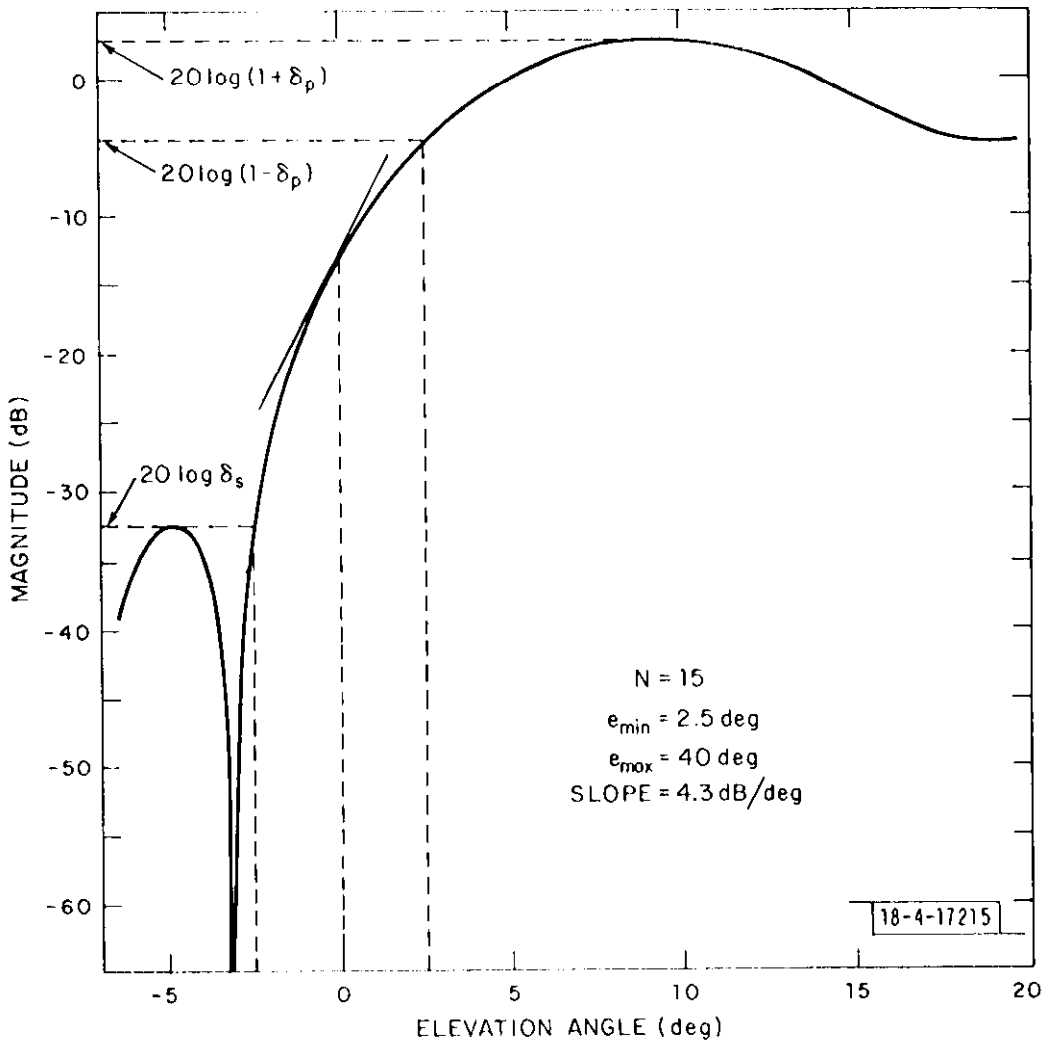

Fig. 10. Subarray antenna pattern (near horizon).

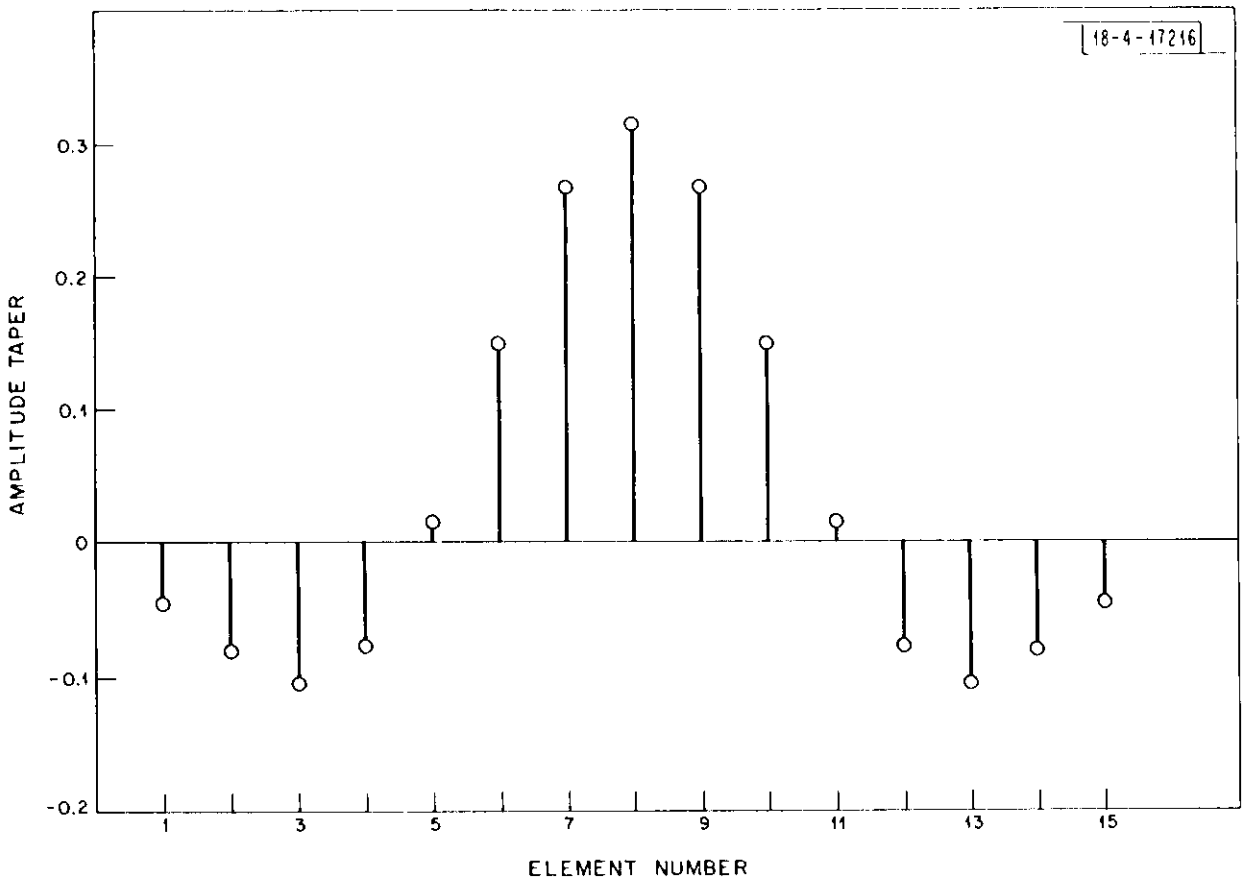

Fig. 11. Optimum antenna pattern amplitude taper.

5.0 Conclusions

A synthesis technique has been developed that performs an optimum tradeoff between the subarray aperture and the base line separation of a two-element interferometer. Receiver noise, hardware phase detector errors, and ground reflection multipath are simultaneously taken into account in the algorithm in order to obtain a specified elevation angle estimation accuracy. Each antenna pattern in the class over which the search was performed was the elevation domain analog of an optimum finite impulse response, linear phase digital filter. They could therefore be directly synthesized using a design algorithm developed by Parks and McClellan. The optimum designs were found to be functions of the maximum elevation angle (i.e., the pass-band edge of the analogous digital filter). For the example studied, it was fortuitous that the specified coverage corresponded to a stationary point; hence the antenna pattern corresponded to an equiripple filter. The same result could therefore have been obtained using the Hofstetter, Oppenheim, and Siegal algorithm [Ref. 9], although the actual algorithm specifications are not as straightforward as with the Parks, McClellan algorithm. Furthermore, the latter technique produces the best designs for any coverage condition, which could be important in some applications.

The synthesis method was used for an example that typifies the requirements for an elevation sensor that provides ground derived elevation data for landing aircraft. For 2.5° to 40° coverage, it was determined that two 7-wavelength antennas spaced 8 wavelengths apart would support 1-milliradian elevation angle errors. In its present form, the antenna pattern design applies a uniform constraint on the magnitude of the sidelobes in the multipath region. As a result of the fact that the multipath reflection coefficient decreases in magnitude for aircraft at higher elevation angles, additional degrees of freedom can be introduced in the optimization by applying a sidelobe constraint function that increases in proportion with the decrease in the reflection coefficient. This alteration can be incorporated into the filter synthesis computer program with little difficulty.

Another possibility for further reducing the subarray aperture is to use the antenna synthesis technique proposed by Evans [Ref. 6], which seeks the minimum phase taper rather than the linear phase taper considered in this report. There is some indication that fewer elements are required to obtain the same antenna pattern specifications.

There remains the issue of ambiguity resolution which always arises in conjunction with the use of an interferometer. This is derived from the fact that more than one cycle of phase is traversed whenever the elevation angle increases by more than $\sin^{-1} D_B$. For the example, it was found that $D_B = 8$ wavelengths; hence, the unambiguous region extends from only 0 to 7.2°. As a consequence that coverage from 2.5° to 40° was desired, there will be five ambiguity lobes that must be resolved. In Part II of this report, this problem is examined from a point of view of the statistical decision theory to determine an optimum strategy for resolving the ambiguities.

PART II

OPTIMUM ANTENNA DESIGN FOR AMBIGUITY RESOLUTION

1.0 Introduction

In Part I of this Technical Note, a design algorithm was developed that could be used to find the optimum tradeoff between the subarray aperture and the interferometer base line for a sensor that would estimate elevation angle to some requisite accuracy. A design for a typical terminal Air Traffic Control application was given in which it was found that errors less than 1 milliradian could be obtained using 7-wavelength antennas spaced 8 wavelengths apart. As a result of the fact that the angle estimate is based on a measurement of the relative phase between the two antennas, ambiguous angle estimates occur whenever the elevation angle is greater than 7.2°. As a result of the fact that coverage is usually desired over a much wider region, typically up to 40°, it is clear that an additional antenna complex will be needed to resolve the ambiguities.

If only phase comparison data are available, ad hoc solutions to the ambiguity resolution problem already exist [Ref. 10]. These schemes usually require that the elemental antennas have enough vertical aperture to provide some discrimination against multipath. An alternative scheme is to use very simple dipole antennas and measure the amplitude and phase of the incident signals. In this way the multipath discrimination can be obtained by properly designing the array antenna pattern. This approach appears to have received no attention in the literature and will therefore be the subject of this report. It will be shown that the ambiguity resolution problem can be formulated as an M-ary hypothesis-testing problem for which the optimum solution can be obtained using statistical decision theory. Bounds, on the probability that receiver noise and multipath cause an ambiguity error, are calculated. As in Part I, the design of an elevation sensor is considered in detail. The performance bounds are evaluated for ground reflection multipath and used as a guide in the selection of the number of additional antennas needed and the inter-element spacings. It is

shown that the probability of an ambiguity error for a 4-element nonuniform array, with antenna elements located at 0.0, 3.2, 6.4, and 11.2 wavelengths, is less than .004.

2.0 Mathematical Formulation

It is assumed that N antenna elements, which are located at positions d_n/λ wavelengths from the bottom antenna, are available, where n = 0, 1, . . . , N - 1, and $d_0 = 0$ as indicated in Fig. 12. Provisions have been made to measure the amplitude and phase at the outputs of each of these antennas. These outputs can be modeled as

$$r_n = A \exp j[\varphi + 2\pi(d_n/\lambda) \sin e] + w_n \tag{1}$$

where, in the simplest case, the only form of interference is caused by the receiver noise, denoted w_n. This is a zero mean complex, white, Gaussian random process with variance

$$\overline{|w_n|^2} = 2\sigma^2 .$$

Letting $\gamma = A \exp j \varphi$ denote the unknown complex amplitude of the received signal; $t_n = d_n/\lambda$, the element spacing in wavelengths and $\upsilon = \sin e$, the direction cosine of the elevation angle e, equation (1) can be written as

$$r_n = \gamma \exp j(2\pi t_n \upsilon) + w_n \quad . \tag{2}$$

For a two-element array, of the type studied in Part I, the data are

$$\begin{aligned} r_0 &= \gamma + w_0 \\ r_1 &= \gamma \exp j(2\pi T\upsilon) + w_1 \end{aligned} \tag{3}$$

where $T = t_N = D/\lambda$ measures the total aperture width in wavelengths. Hofstetter and Delong [Ref. 11] have shown that the optimum estimate of υ is

$$\hat{\upsilon} = (\arg r_1 - \arg r_0)/2\pi T \tag{4}$$

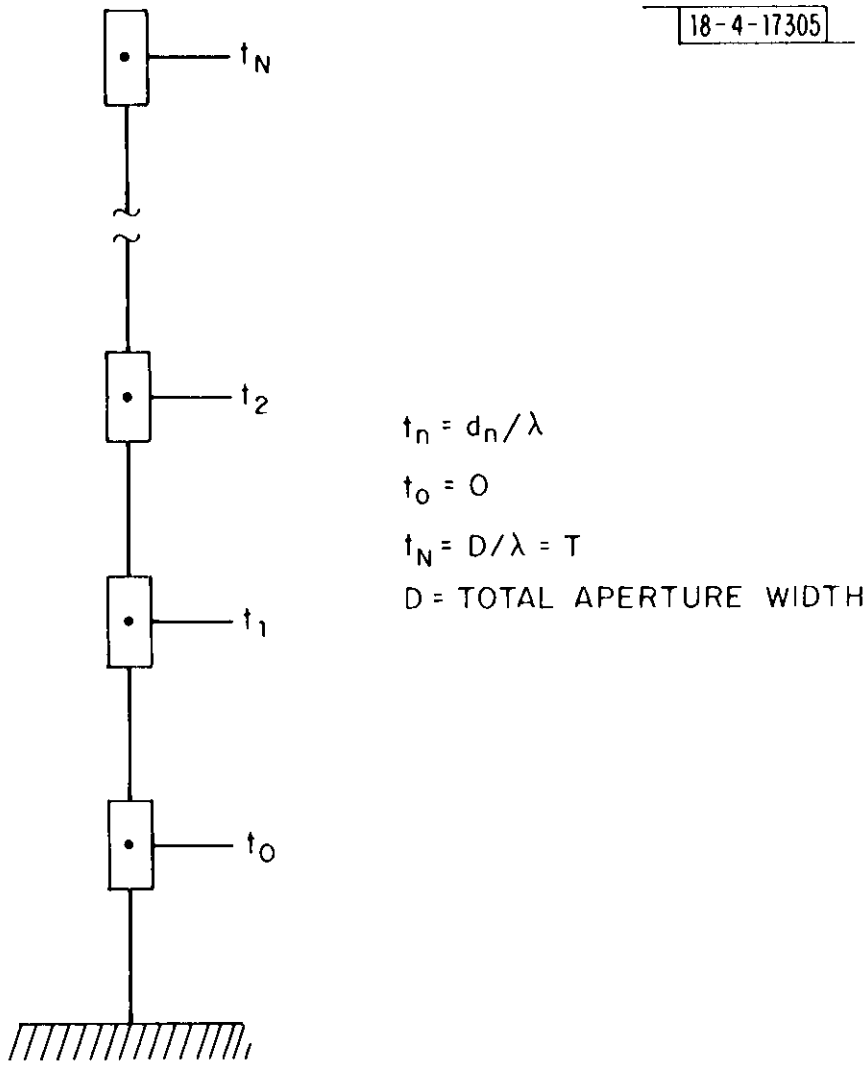

Fig. 12. Antenna configuration for ambiguity resolution.

which is the interferometer or phase comparison monopulse solution. The data in equation (3) and the estimate in equation (4) are ambiguous whenever υ increases by more than $1/T$. For coverage over an angular region from 0 to e_{max}, the direction cosine varies from 0 to υ_{max}, (= $\sin e_{max}$), which in many applications is larger than $1/T$, resulting in ambiguous data. In fact, the elevation pattern of the interferometer will have $M = [\upsilon_{max}/T]_+$ ambiguity lobes, where $[x]_+$ denotes the smallest integer $\geq x$. In order to make the ambiguity lobe dependence clear, it is useful to express the parameter υ in the following way

$$\upsilon = \upsilon_0 + \frac{m}{T} \tag{5}$$

where $0 \leq \upsilon_0 \leq 1/T$ denotes the relative position of υ as it would appear in the principal ambiguity lobe from 0 to $1/T$, while m/T (m some integer from 0 to $M - 1$) locates the ambiguity lobe in which the true parameter value is located. It follows, therefore, that the two-element interferometer is capable of estimating only the local part of υ, namely υ_0. This estimate will be denoted as $\hat{\upsilon}_0$ and is determined from equation (4), viz

$$\hat{\upsilon}_0 = (\arg r_1 - \arg r_0)/2\pi T \quad . \tag{6}$$

In Part I, the design of the two-element interferometer was considered in detail. Basically it was established that it was possible to construct an antenna pair having the smallest possible subarray aperture and interferometer base line to achieve a prescribed error in the estimate of υ_0. This error is usually quite small (~ 1 milliradian); hence, if the correct ambiguity lobe were known (e. g., $\hat{m}$), a very accurate estimate of υ could be obtained simply by taking $\hat{\upsilon} = \hat{\upsilon}_0 + \hat{m}/T$. The problem is in the determination of m, which is known only to be some integer from 0 to $M - 1$. Two antennas are clearly insufficient for the determination of m, hence, additional elements must be provided for this purpose. In fact, it is proposed that a separate antenna complex be used to perform this function, thus separating the local estimation and ambiguity resolution functions in practice

as well as in concept. The two-element interferometer yields the estimate $\hat{\upsilon}_0$, which is very close to the true parameter value, υ_0. Therefore, there are M possible values for the estimate of υ:

$$\hat{\upsilon}_0$$

$$\hat{\upsilon}_0 + 1/T$$

$$\hat{\upsilon}_0 + 2/T$$

$$\vdots$$

$$\hat{\upsilon}_0 + (M - 1)/T \quad .$$

The problem of determining which integer value to choose can be formulated as an M-ary hypothesis test in which the m^{th} hypothesis is

$$H_m: \ \hat{\upsilon}_m = \hat{\upsilon}_0 + m/T \quad m = 0, 1, \ldots, M - 1 \quad . \tag{7}$$

Using the data vector $\underline{r} = \text{col}(r_0, r_1, r_2, \ldots, r_{N-1})$, where r_n is given by equation (2), it is desired to decide in favor of one of the M hypotheses. As a result of the fact that the aircraft for which the elevation angle is being estimated is equally likely to be anywhere within the proposed airspace, the Bayes rule that leads to the minimum probability of erroneously selecting the wrong hypothesis (i.e., ambiguity lobe) is given by [Ref. 12]: declare H_m if, and only if

$$p(\underline{r}|H_m) > p(\underline{r}|H_k) \quad k = 0, 1, \ldots, M - 1; \ k \neq m, \tag{8}$$

where $p(\underline{r}|H_k)$ is the probability density function of the random vector $\underline{r}$ under the assumption that the k^{th} hypothesis is true. As a result of the fact that the noise terms in equation (2) are Gaussian, this density function is easily computed. In fact, the likelihood function can be shown to be given by

$$\ell(k) = \left| \sum_{n=0}^{N-1} \left\{ r_n \exp\left[-j\, 2\pi \left(\hat{\upsilon}_0 + \frac{k}{T} \right) t_n \right] \right\} \right|^2 \quad . \tag{9}$$

The optimum test declares in favor of hypothesis H_m if, and only if, $\ell(m) > \ell(k)$, $k = 0, 1, \ldots, M-1$; $k \neq m$. In practical terms, the processor scans the antenna pattern to the M beam positions, $\hat{\upsilon}_0 + k/T$, $k = 0, 1, \ldots, M-1$, and chooses the beam position for which the power measured is largest. It is important to note that the scanning is actually done in software, with the antenna elements being entirely passive.

It will be useful to simplify the notation for the test statistic in equation (9). Signals are defined by the vectors $\underline{s}(\hat{\upsilon}_k) = \mathrm{col}[s_0(\hat{\upsilon}_k), s_1(\hat{\upsilon}_k), \ldots, s_{N-1}(\hat{\upsilon}_k)]$,
where

$$s_n(\upsilon) = \exp j\, 2\pi \upsilon t_n \quad . \tag{10}$$

Using the inner product notation, $< \underline{x}, \underline{y} > = \frac{1}{N} \sum_{n=0}^{N-1} x_n y_n^*$, the test statistic can then be written as

$$\ell(k) = \left| < \underline{r}, \underline{s}(\hat{\upsilon}_k) > \right|^2 \quad . \tag{11}$$

In Section 3.0, this expression is used in the development of a bound on the probability of an ambiguity error as a result of the presence of receiver noise and multipath.

3.0 Error Performance

Using Bayes' rule, the probability that the receiver declares the incorrect ambiguity lobe is

$$P(\epsilon) = \int P(\epsilon | e_s)\, p(e_s)\, de_s \tag{12}$$

where e_s is the true elevation angle of the aircraft, and $p(e_s)$ represents the probability density function or the relative weighting to be given to that elevation angle. Although the value of the average probability may be of some interest, it is standard practice to base the design of an Air Traffic Control sensor on the worst case condition. This is especially important for a landing monitor in view of the fact that an aircraft will maintain a fixed elevation angle for a relatively long period of time. It is also important that the probability of an ambiguity error be low during that time segment. Therefore, the effort will concentrate on the development of the conditional error probability $P(\epsilon | e_s)$. To put the conditional event into the decision theoretical framework, the following definitions are needed:

$$\upsilon_s = \sin e_s \tag{13a}$$

$$m = [T \upsilon_s]_- \tag{13b}$$

$$\upsilon_0 = \upsilon_s - \frac{m}{T} \tag{13c}$$

where $[x]_-$ the largest integer $\leq x$. Then the direction cosine of the true aircraft elevation angle can be written as

$$\upsilon_s = \upsilon_0 + \frac{m}{T} \tag{14}$$

whence, m can be interpreted as the true ambiguity lobe.

The estimate of v_0, $\hat{v}_0$, is developed at the output of the phase comparison monopulse system. The estimate of the m^{th} ambiguity lobe, $\hat{m}$, is obtained by selecting the largest of the M values of the likelihood function, $\ell(k)$, given in equations (9) and (11). An ambiguity error is made if, and only if, $\ell(k) > \ell(m)$ for some value of k not equal to m. Therefore, the conditional probability of error is given by

$$P(\epsilon | e_s) = P\Big[\ell(0) > \ell(m) \cup \ell(1) > \ell(m) \ldots \ell(m-1) > \ell(m) \cup \ell(m+1) > \ell(m)$$

$$\ldots \ell(M-1) > \ell(m) \,\Big|\, v_s = v_0 + \frac{m}{T}\Big] \qquad (15)$$

where $A \cup B$ denotes the logical "and/or" union of two events, A and B. In general $\ell(0), \ell(1) \ldots, \ell(M-1)$ are correlated random variables that render equation (15) difficult to evaluate analytically. There is a strong parallel between the problem of ambiguity resolution and M-ary digital communications. The so-called union bound has been usefully applied to the latter problem [Ref. 13], and it is reasonable to attempt its application to the problem at hand.

3.1 The Union Bound

Applied to equation (15), the union bound is simply

$$P(\epsilon | e_s) \leq \sum_{\substack{k=0 \\ k \neq m}}^{M-1} P\Big[\ell(k) > \ell(m) \,\Big|\, v_s = v_0 + \frac{m}{T}\Big] \quad . \qquad (16)$$

The probability expression in equation (16) is more likely to be analytically tractable because it only involves a bivariate distribution. In particular, it is necessary to evaluate the joint probability density function (pdf) for the random variables, $\ell(k)$ and $\ell(m)$, defined by equation (11). Equation (11) and the associated decision criterion represented an optimum receiver configuration when the interference was receiver noise. This processor is to be

used when multipath signals are also present. Therefore, the statistical description of the random variable, $\ell(m)$, will be derived for a received signal that includes the direct and multipath data. In this case, the received data vector $\underline{r}$ has components

$$r_n = \gamma_s \exp j2\pi \upsilon_s t_n + \gamma_I \exp j2\pi \upsilon_I t_n + w_n$$

$$= \gamma_s s_n(\upsilon_s) + \gamma_I s_n(\upsilon_I) + w_n \qquad (17)$$

where $\gamma_s = A_s \exp j\varphi_s$, $\gamma_I = A_I \exp j\varphi_I$ represent the complex amplitudes of the direct multipath waveforms, and $\upsilon_s = \sin e_s$, $\upsilon_I = \sin e_I$ represent the direction cosines of the direct and multipath signals, respectively. Using equation (10), the data vector can then be written as

$$\underline{r} = \gamma_s \underline{s}(\upsilon_s) + \gamma_I \underline{s}(\upsilon_I) + \underline{w} \quad . \qquad (18)$$

The test statistics can then be evaluated by substituting this result into equation (11). The result is

$$\ell(k) = \left| \gamma_s < \underline{s}(\upsilon_s), \ \underline{s}(\hat{\upsilon}_k) > + \gamma_I < \underline{s}(\upsilon_I), \ \underline{s}(\hat{\upsilon}_k) > + < \underline{w}, \ \underline{s}(\hat{\upsilon}_k) \right|^2 \qquad (19)$$

where $\hat{\upsilon}_k = \hat{\upsilon}_0 + k/T$. A similar expression holds for $\ell(m)$.

It is appropriate to introduce the signal correlation coefficient

$$\lambda(\upsilon) = \frac{1}{N} \sum_{n=0}^{N-1} \exp j2\pi \upsilon t_n \quad . \qquad (20)$$

This function can be interpreted as the array factor or antenna pattern of the array of antenna elements. It is the design of this function that is controlled by choosing the inter-element spacings, $t_0, t_1, \ldots, t_{N-1}$. It will now be

shown that the probability of error performance depends almost entirely on the shape of this function.

By definition of the inner products used in equation (19), it follows that

$$< \underline{s}(\upsilon_1), \underline{s}(\upsilon_2) > = \lambda(\upsilon_1 - \upsilon_2) \quad . \tag{21}$$

Therefore, equation (19) can be written as

$$\ell(k) = \left| \gamma_s \lambda(\upsilon_s - \hat{\upsilon}_k) + \gamma_I \lambda(\upsilon_I - \hat{\upsilon}_k) + \eta(k) \right|^2 \tag{22}$$

where $\eta(k) = < \underline{w}, \underline{s}(\hat{\upsilon}_k) >$ is a zero mean, complex Gaussian random variable. Its variance is given by the expressions

$$\overline{|\eta(k)|^2} = 2\sigma^2 N \tag{23a}$$

$$\overline{\eta^2(k)} = 0 \tag{23b}$$

which follow from the fact that w_n is a white noise sequence. Similarly, it follows that

$$\ell(m) = \left| \gamma_s \lambda (\upsilon_s - \hat{\upsilon}_m) + \gamma_I \lambda(\upsilon_I - \hat{\upsilon}_m) + \eta(m) \right|^2 \tag{24}$$

where $\eta(m)$ is also a zero mean complex Gaussian random variable with the variance given in equation (23). In addition, $\eta(k)$ and $\eta(m)$ have covariance given by

$$\overline{\eta(k)\,\eta^*(m)} = \frac{2\sigma^2}{N} \lambda(\upsilon_m - \hat{\upsilon}_k) \tag{25a}$$

$$\overline{\eta(k)\eta(m)} = 0 \quad . \tag{25b}$$

It is possible to obtain an expression for the joint pdf for $\ell(m)$ and $\ell(k)$, but the final result is complicated and does not lead to mathematically tractable results. In lieu of the rigorous approach, a first-order analysis is performed, which approximates $\ell(k)$ and $\ell(m)$ as correlated Gaussian random variables. The approximation is quite accurate whenever the effective signal-to-noise ratio is greater than 12 dB, which will certainly be the case for the problem at hand. The details are quite straightforward and hence have been relegated to the Appendix. It is shown that the upper bound for the conditional probability of error is

$$P\left(\epsilon \,|\, \upsilon_s = \upsilon_o + \frac{m}{T}\right) \leq \sum_{\substack{k=0 \\ k\neq m}}^{M-1} \operatorname{erfc}\left[\chi_{mk}(\rho, \varphi)\right] \tag{26}$$

where

$$\operatorname{erfc}(x) = \frac{1}{\sqrt{2\pi}} \int_x^\infty e^{-1/2\, t^2} \tag{27}$$

$$\chi_{mk}(\rho, \varphi) = \frac{1}{\sqrt{2}} \left(\frac{N|\gamma_s|^2}{2\sigma^2}\right)^{1/2} \frac{|\xi(m)|^2 - |\xi(k)|^2}{\left\{|\xi(m)|^2 + |\xi(k)|^2 - 2\,\mathrm{Re}\left[\xi(m)\xi^*(k)\lambda\left(\frac{m-k}{T}\right)\right]\right\}^{1/2}} \tag{28}$$

$$\xi(m) = \lambda\left[\upsilon_s - \left(\hat{\upsilon}_0 + \frac{m}{T}\right)\right] + \lambda\left[\upsilon_I - \left(\hat{\upsilon}_0 + \frac{m}{T}\right)\right]\rho \exp j\varphi \tag{29a}$$

$$\xi(k) = \lambda\left[\upsilon_s - \left(\hat{\upsilon}_0 + \frac{k}{T}\right)\right] + \lambda\left[\upsilon_I - \left(\hat{\upsilon}_0 + \frac{k}{T}\right)\right]\rho \exp j\varphi \tag{29b}$$

and where the complex reflection coefficient is

$$\rho \exp j\varphi = \frac{\gamma_I}{\gamma_s} \tag{30}$$

In equation (30), ρ represents the magnitude of the multipath reflection coefficient, and φ represents the relative phase between the direct and multipath signals. The purpose of including ρ and φ in the argument of the erfc function, equations (26) and (28), is to make clear the implicit dependence on these important parameters. It is also interesting to note that the performance depends critically on the configuration of the antenna array through the array factor $\lambda(\upsilon)$.

3.2 Special Case: No Multipath

When the multipath signal is absent, $\rho = 0$; and because $\upsilon_s = \upsilon_0 + \frac{m}{T}$, equation (29) reduces to

$$\xi(m) = \lambda(\upsilon_0 - \hat{\upsilon}_0) \tag{31a}$$

$$\xi(k) = \lambda\left(\upsilon_0 - \hat{\upsilon}_0 + \frac{m - k}{T}\right) \quad . \tag{31b}$$

The term, $\upsilon_0 - \hat{\upsilon}_0$, represents the error in the estimate of the direction cosine as generated by the associated interferometer. For a well designed system, this error is small enough that the following approximations hold:

$$\xi(m) = \lambda(\upsilon_0 - \hat{\upsilon}_0) \approx 1 \tag{32a}$$

$$\xi(k) = \lambda\left(\upsilon_0 - \hat{\upsilon}_0 + \frac{m - k}{T}\right) \approx \lambda\left(\frac{m - k}{T}\right) \quad . \tag{32b}$$

In this case, the conditional probability of error reduces to

$$P\left(e \,\middle|\, \upsilon_s = \upsilon_0 + \frac{m}{T}\right) \leq \sum_{\substack{k=0 \\ k \neq m}}^{M-1} \operatorname{erfc}\left\{\sqrt{\frac{N\alpha}{2}\left[1 - \left|\lambda\left(\frac{m-k}{T}\right)\right|^2\right]}\right\} \tag{33}$$

where

$$\alpha = \frac{|\gamma_s|^2}{2\sigma^2} \tag{34}$$

is the signal-to-noise ratio at each antenna element. The result is intuitively satisfying in the sense that it shows that the probability of error decreases with increasing signal-to-noise ratio and decreasing sidelobe levels in the array antenna pattern. For a uniformly spaced array, $t_n = n\,\Delta$, $(N-1)\Delta = T$,

$$\lambda(\upsilon) = \frac{\sin(\pi N \Delta \upsilon)}{N \sin(\pi \Delta \upsilon)} \exp[j\,\pi\,(N-1)\,\Delta\,\upsilon] \quad . \tag{35}$$

Therefore, as long as $\Delta^{-1} \geq \sin e_{max}$, where e_{max} is the maximum elevation angle, then the grating lobe will occur outside the desired coverage region, and it follows that

$$\left|\lambda\left(\frac{m-k}{T}\right)\right| \approx 0, \quad .$$

Hence, the probability of an ambiguity error is

$$P\left(\epsilon \,\middle|\, \upsilon_s = \upsilon_0 + \frac{m}{T}\right) \leq (M-1)\,\mathrm{erfc}\left(\sqrt{\frac{N\alpha}{2}}\right) \tag{36}$$

which represents the smallest upper bound that can be derived. In this sense, the uniform array is optimum.

3.3 General Case

In the general case, in which multipath signals are present, the performance depends not only upon the array antenna pattern and signal-to-noise ratio; but upon the magnitude and phase of the reflection coefficient as well. At any one aircraft position, the relative phase is likely to assume any value from 0 to 2π. However, a change in phase can occur only when the path

length difference between the direct and multipath signals changes measurably, which requires a significant displacement in the position of the aircraft. As a result of this fact, the value of the relative phase may not change over relatively long periods of time. From a design point of view, this means that the performance bound should be evaluated at the worst case phase. Therefore, the conditional probability of error, equation (26), is further upper bounded by

$$P\left(\epsilon \mid v_s = v_0 + \frac{m}{T}\right) \leq \max_{0 \leq \varphi < 2\pi} \sum_{\substack{k=0 \\ k \neq m}}^{M-1} \operatorname{erfc}[\chi_{mk}(\rho, \varphi)] \quad . \quad (37)$$

This bound depends on only the magnitude of the reflection coefficient, which, in the case of an azimuth sensor or an elevation sensor in front of hilly terrain, is difficult to model. In these cases, an evaluation of the probability of error performance will depend on reasonable estimates for the values that this parameter could take on.

3.4 Special Case: Multipath as a Result of a Flat Earth

In many cases of practical interest, it can be assumed that the area in front of an elevation sensor is flat. For these situations, models exist that characterize the reflection coefficient as a function of elevation angle. For vertical polarization, which typifies the elevation sensor design, the magnitude of the reflection coefficient for an angle of incidence, e_I, is given by

$$\rho(e_I) = \frac{\epsilon_r \sin e_I - (\epsilon_r - \cos^2 e_I)^{1/2}}{\epsilon_r \sin e_I + (\epsilon_r - \cos^2 e_I)^{1/2}} \quad (38)$$

where $\epsilon_r = \epsilon' - j\epsilon''$ is the complex dielectric constant of the reflecting terrain. Most references give data for the earth in terms of the relative dielectric

constant, ϵ/ϵ_0 (where ϵ = dielectric constant, and ϵ_0 = dielectric constant of the space) and conductivity, σ, which are related to ϵ' and ϵ'' by [Ref. 14].

$$\epsilon' = \epsilon/\epsilon_0 \tag{39a}$$

$$\epsilon'' = 60\,\lambda\,\sigma \tag{39b}$$

where λ is the wavelength in meters, and σ the conductivity in mhos/meter. Using these expressions, the reflection coefficients for dry land and grass, which represent extreme cases, are plotted in Fig. 13. For an aircraft at long range (> 1 mile), the angle of incidence will be equal to the elevation angle of the aircraft, e_s. Therefore, the magnitude of the reflection coefficient can be written explicitly in terms of e_s, namely $\rho(e_s)$. This, in turn, renders the upper bound on the error probability a function of only the aircraft elevation angle. Summarizing these results, it is found that for flat terrain, the probability of an ambiguity error for an elevation sensor for an aircraft at elevation angle e_s is given by the equations

$$P\left(\epsilon \,\middle|\, \upsilon_s = \upsilon_0 + \frac{m}{T}\right) \leq \max_{0 \leq \varphi < 2\pi} \sum_{\substack{k=0 \\ k \neq m}}^{M-1} \operatorname{erfc}\{\chi_{mk}[\rho(e_s),\ \varphi]\} \tag{40}$$

$$\upsilon_s = \sin e_s \tag{41a}$$

$$m = [T\,\upsilon_s]_- \tag{41b}$$

$$\upsilon_0 = \upsilon_s - \frac{m}{T} \tag{41c}$$

$$\chi_{mk}[\rho(e_s), \varphi] = \left(\frac{N\alpha}{2}\right)^{1/2} \frac{|\xi(m)|^2 - |\xi(k)|^2}{\left\{|\xi(m)|^2 + |\xi(k)|^2 - 2\,R_e\left[\xi(m)\xi^*(k)\lambda\left(\frac{m-k}{T}\right)\right]\right\}^{1/2}} \tag{42}$$

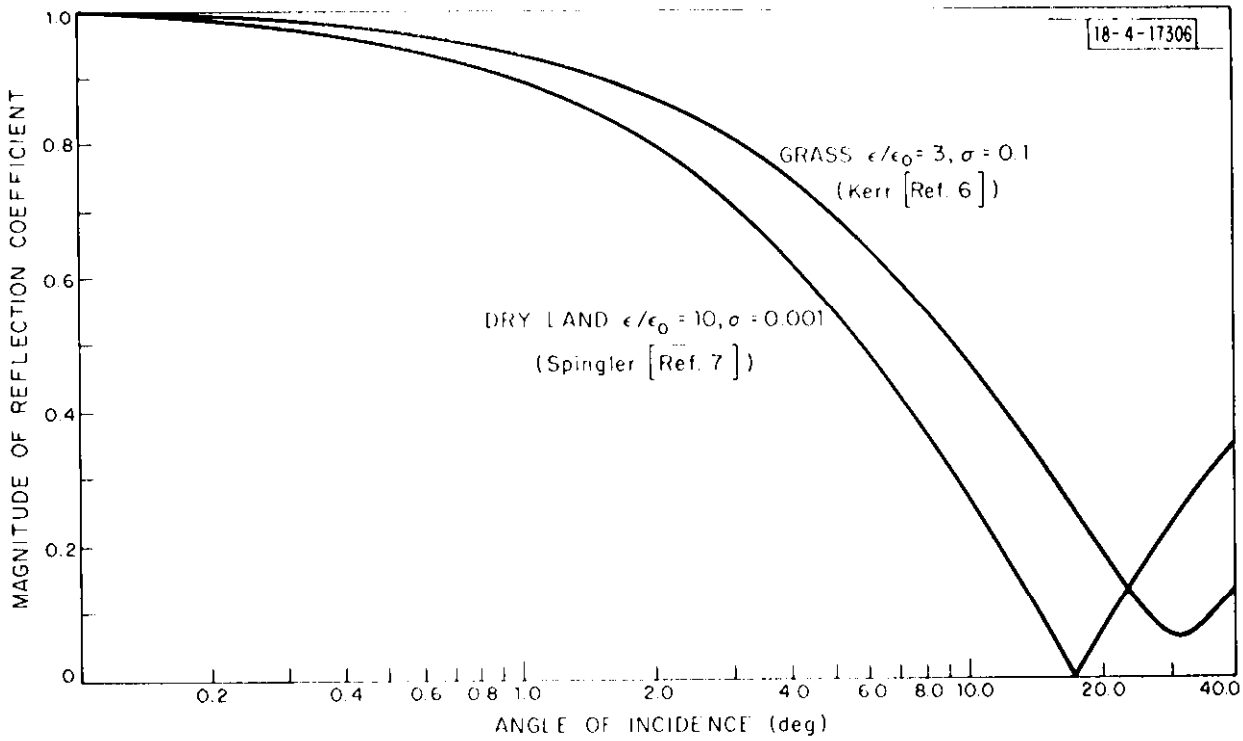

Fig. 13. Reflection coefficient at L-band.

$$\xi(k) = \lambda\left[\upsilon_s - \left(\upsilon_0 + \frac{k}{T}\right)\right] + \lambda\left[\upsilon_I - \left(\hat{\upsilon}_0 + \frac{k}{T}\right)\right]\rho(e_s)\exp j\varphi \qquad (43)$$

$$\lambda(\upsilon) = \frac{1}{N}\sum_{n=0}^{N-1} \exp j 2\pi\upsilon T_n \qquad (44)$$

$$\rho(e_s) = \frac{\epsilon_r \sin e_s - (\epsilon_r - \cos^2 e_s)^{1/2}}{\epsilon_r \sin e_s + (\epsilon_r - \cos^2 e_s)^{1/2}} \qquad (45)$$

These equations are easily programmed for numerical evaluation. Except for the elevation angle, the only additional parameter to be specified is α, the signal-to-noise at each antenna element in the array. A power budget estimate was made in Part I, Table 2.1, that indicated that the signal-to-noise ratio at the output of each antenna element would be at least 26 dB without including the additional gain caused by the elemental antenna or the loss caused by multipath fading. A simple antenna element might be a dipole on a tri-plane reflector, which would give the desired $\pm 60^\circ$ azimuth and $\pm 40^\circ$ elevation coverage*. Using the formula

$$G_o = 4\pi\left(\frac{50.9}{BW_{az}}\right)\left(\frac{50.9}{BW_{el}}\right) \qquad (46)$$

the elemental antenna gain is estimated to be 5 dB. The necessary margin for a multipath fade is difficult to estimate in this case, because the exact shape of the antenna pattern is unknown. Using Fig. 13 and assuming no multipath attenuation caused by the antenna pattern at 2.5° elevation, the design operating point, the worst case multipath fade could be as great as

*Note that no ground reflection multipath attenuation is postulated for the antenna element.

15 dB. Thereby resulting in an antenna element signal-to-noise ratio of 16 dB. Using this value for α in equation (42), a plot of the probability of an ambiguity error as a function of elevation angle can be generated for a particular antenna array configuration. Specifying the antenna array requires that the number of elements and the inter-element spacings be specified. A number of examples will now be evaluated for various antenna configurations applied to the scenario described in Part I. For that case, elevation angle estimates having 1-milliradian rms error were developed by a phase comparison monopulse system using two 7-wavelength apertures. The phase centers of the apertures were separated by 8 wavelengths. With the interferometer base line, T, equal to 8, it follows that the direction cosine has ambiguities at $m/8$, $m=0, 1, 2, \ldots, M-1$. By definition, $\nu = \sin e$, where e is the elevation angle, whence it follows that the ambiguous regions are 0° -7.18°, 7.18° -14.47°, 14.47° -22.02°, 22.02° -30°, 30° -38.68°. Therefore, the number of ambiguous regions, M, is 5.

The most obvious antenna configuration to select is the uniformly spaced array because its array factor can be written explicitly (i.e., equation (35)), and it has fairly low sidelobes, provided that the grating lobe is outside the 0 to 40° elevation coverage region. This can be assured by selecting the inter-element spacing, Δ, such that $\Delta^{-1} \geq \sin e_{max}$. For the case at hand, $e_{max} = 40^\circ$; whence $\Delta \leq 1.56$. At first it was thought that the grating lobe would also have to be kept outside of the -40° to 0° region of the ground reflected multipath as well, which would have necessitated an inter-element spacing of $\Delta \leq 1.01$. However, as illustrated in Fig. 13, the reflection coefficient is attenuated at these angles as a result of the nature of the reflection process which overcomes the effect of the ambiguous lobe in this region. In order to indicate that this is so, the plots in Figs. 14 through 17 designate the probability of an ambiguity error vs the elevation angle for a uniform array having 4, 5, 6, and 7 antenna elements. For the 4-element array, the mainlobe width is approximately 10.5 degrees. Therefore, when the beam is pointed to the 2.5° elevation angle, the multipath at -2.5° will be within the 3-dB bandwidth of the antenna pattern and, hence, is not attenuated significantly to render the effects of multipath

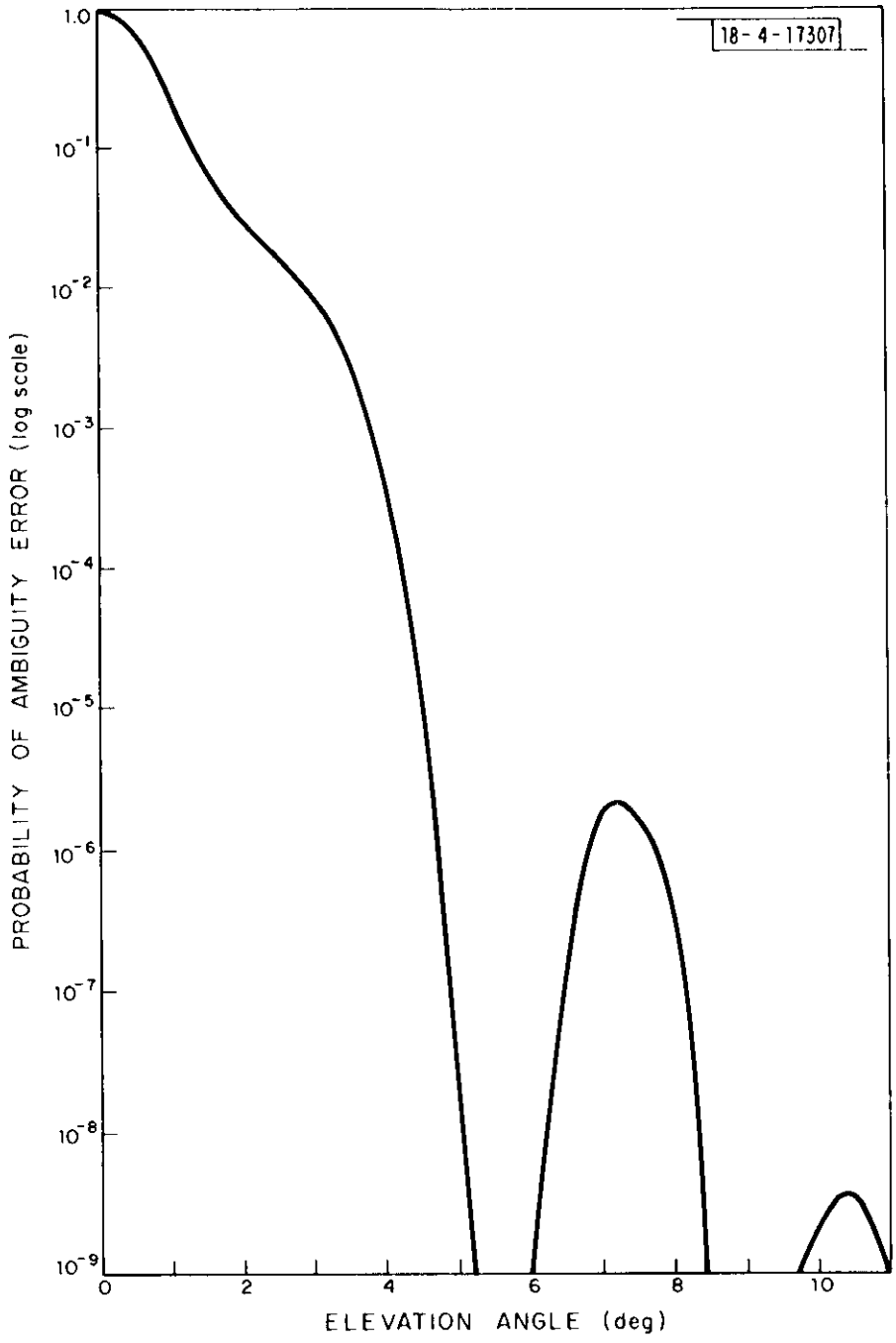

Fig. 14. Upper bound on the probability of an ambiguity error (4-element uniform array).

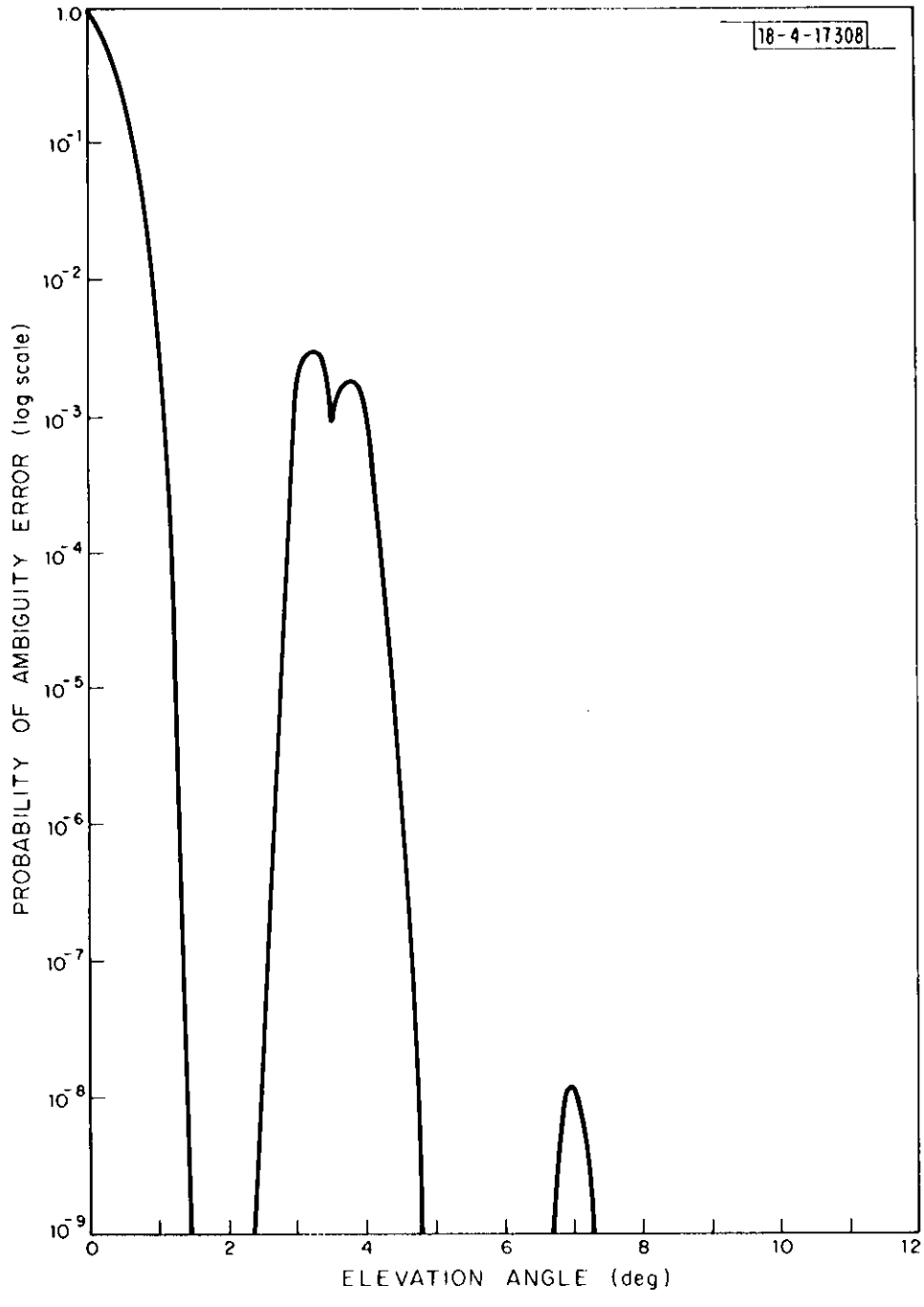

Fig. 15. Upper bound on the probability of an ambiguity error (5-element uniform array).

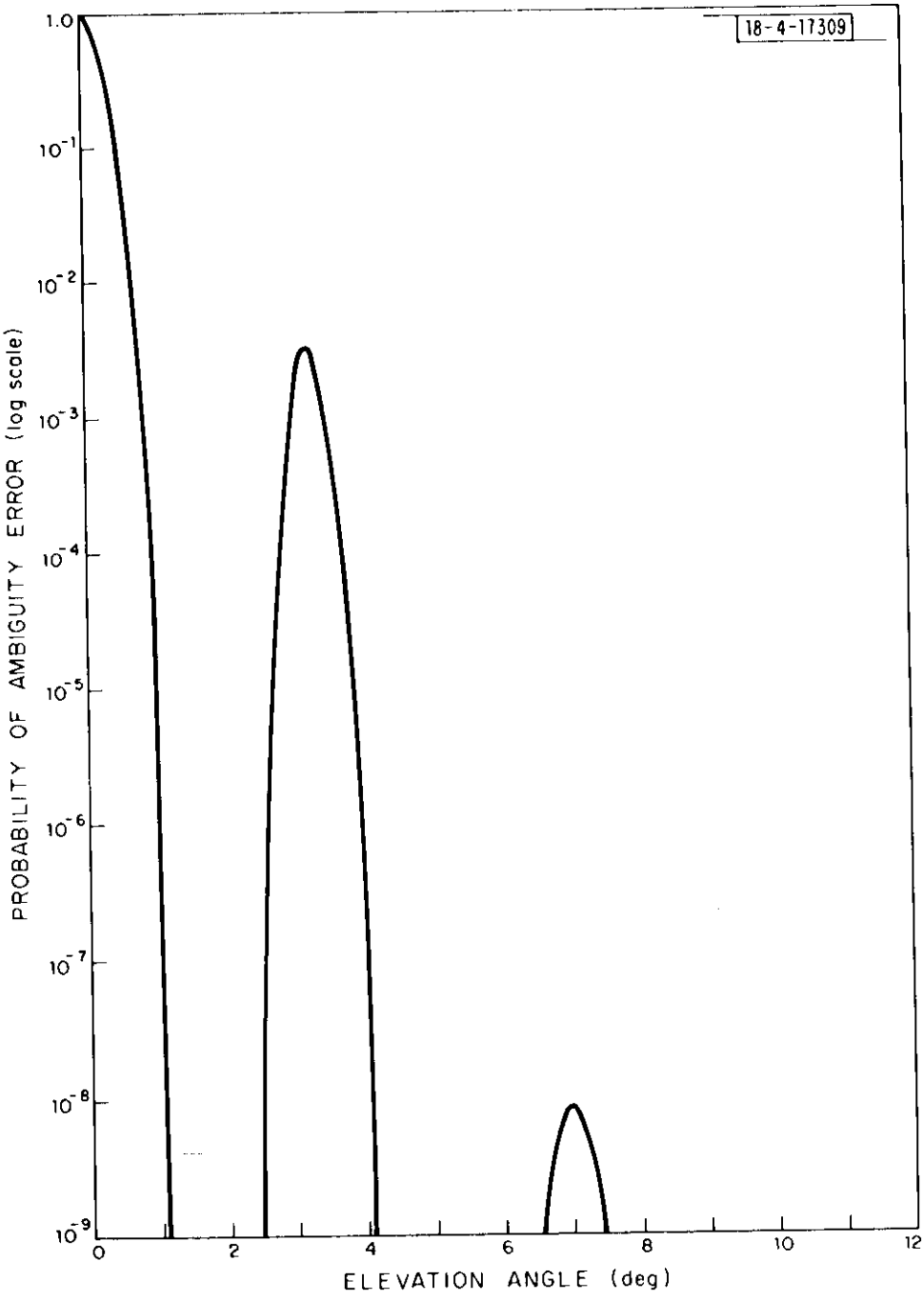

Fig. 16. Upper bound on the probability of an ambiguity error (6-element uniform array).

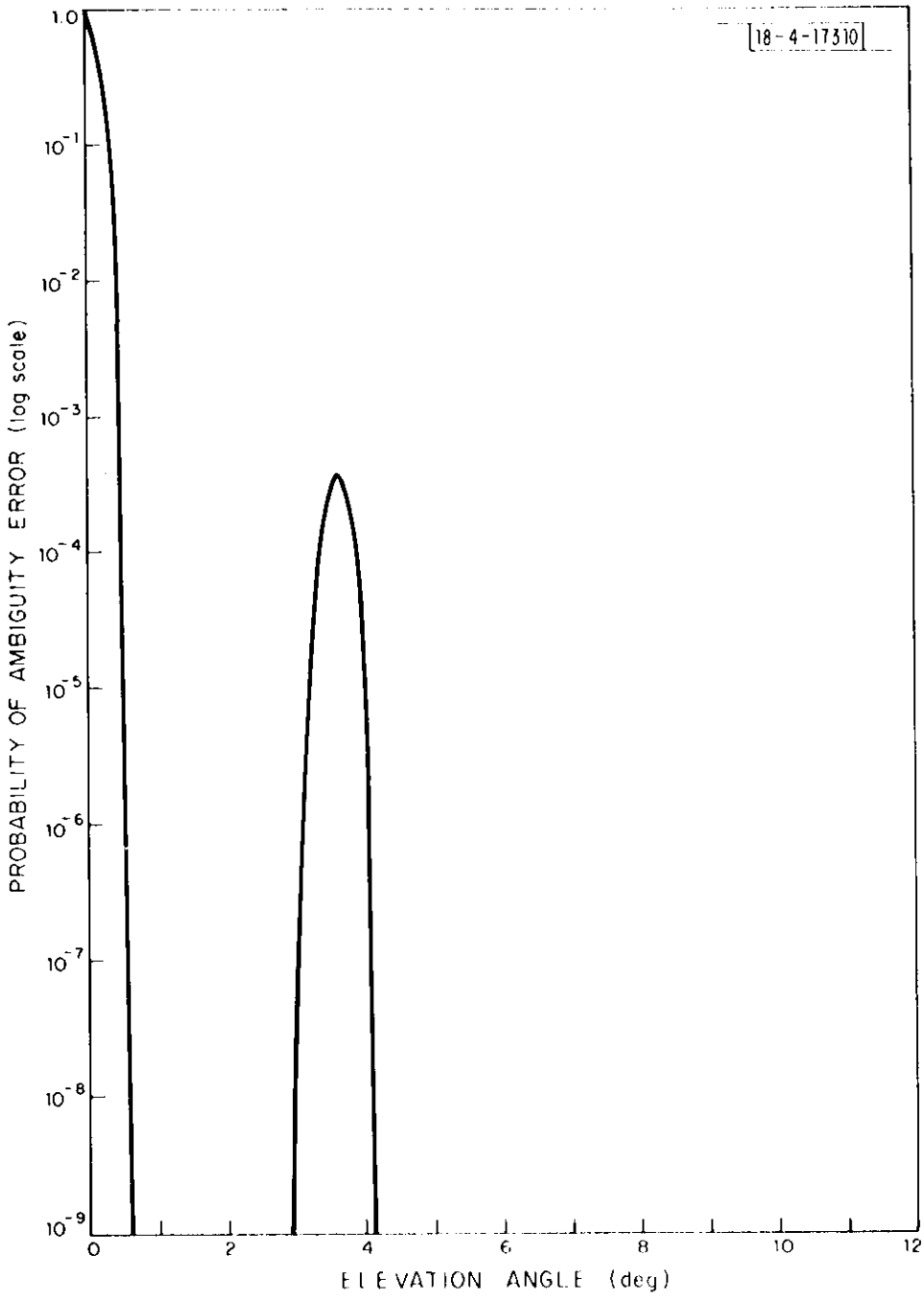

Fig. 17. Upper bound on the probability of an ambiguity error (7-element uniform array).

negligible. This is undoubtedly the reason for the poor performance of the 4-element array at low elevation angles.

The relatively more frequent incidence of errors in the 3^{o} to 4^{o} elevation angle region can be tempered somewhat by the fact that the plot represents an upper bound on performance when the direct and multipath signals maintain their worst case phase relationship. Therefore, the average performance is likely to be significantly better.

In a practical implementation, the cost of the ambiguity resolving array increases with each additional antenna element in view of the fact that in addition to the actual antenna element, an amplitude and phase measurement capability must also be provided. Therefore, there is a premium in trying to keep the number of antenna elements as small as possible. This can be done by using non-uniformly spaced antenna elements. As an example, antennas were located at 0, 3.2, 6.4 and 11.2 wavelengths from the bottom antenna which resulted in the array antenna pattern illustrated in Fig. 18. The corresponding plot of the upper bound of an ambiguity error is illustrated in Fig. 19, which indicates that performance, comparable to the 5-element uniform array, can be obtained. It is likely that even better performance can be obtained by performing a more exhaustive search over all possible spacings for a 4-element array.

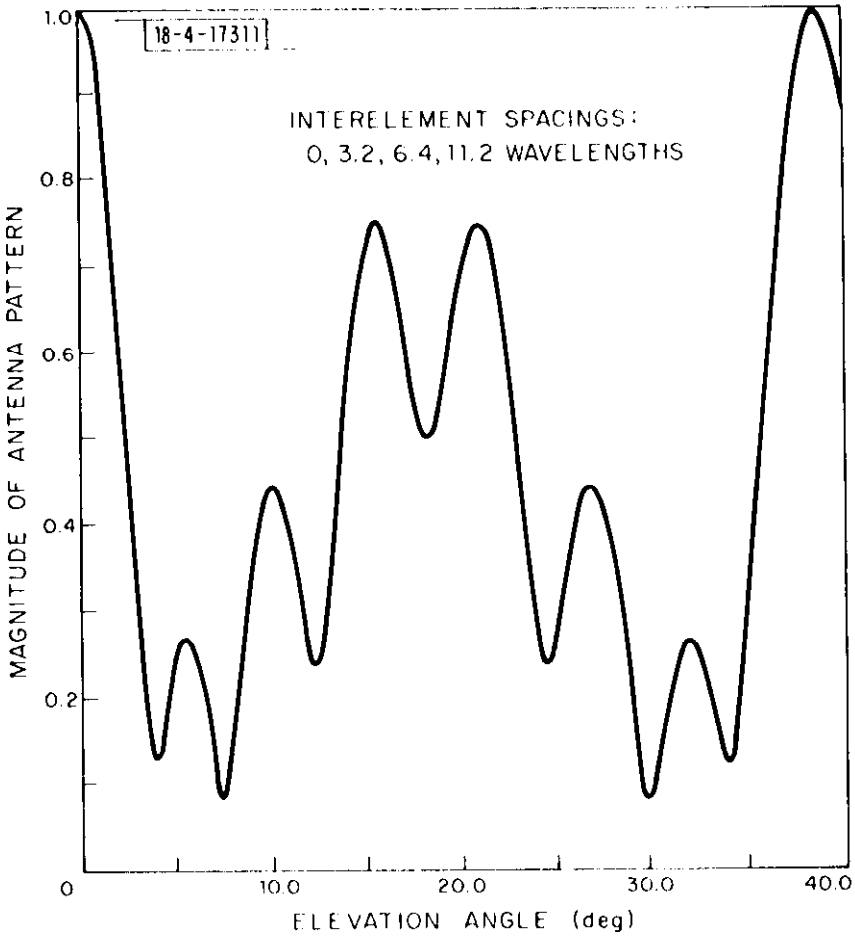

Fig. 18. Antenna pattern of 4-element non-uniformly spaced array.

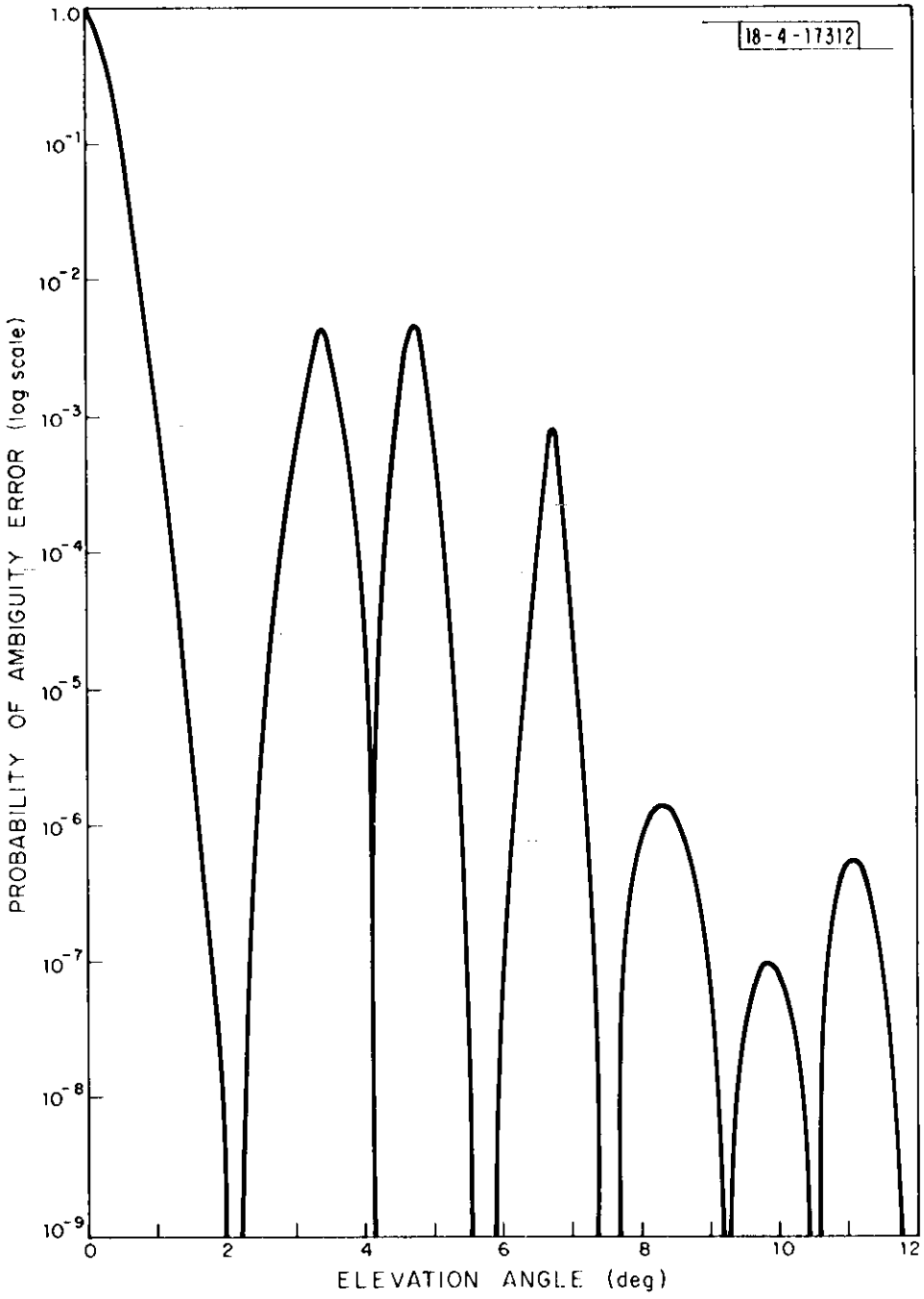

Fig. 19. Upper bound on the probability of an ambiguity error (4-element non-uniform array).

4.0 Conclusions

In Part I of this report an optimum design for a two-element interferometer was developed for an elevation angle sensor. Although capable of generating very accurate elevation angle measurements (~1 milliradian) in the presence of ground reflection multipath, the sensor was intrinsically ambiguous. A separate sensor for resolving the ambiguities was proposed, and a design procedure was developed by formulating the ambiguity resolution problem as an M-ary statistical hypothesis test. A receiver structure resulted that could be interpreted as a beam forming array that scanned the antenna beam to M ambiguous angles, estimating the true angle on the basis of the position that resulted in the largest power. This strategy was optimum for the case of receiver noise interference.

The effects of ground reflection multipath were evaluated by deriving an upper bound on the probability of an ambiguity error. The bound (although a function of the relative phase between the direct and multipath signals) was calculated only at the worst case phase. It was shown that low error probabilities ($< .004$) could be obtained for a 4-element non-uniformly spaced array with relatively inexpensive ($< \$100$) dipole antennas on a tri-plane reflector spaced at 0, 3.2, 6.4, and 11.2 wavelengths. Combined with the two-element interferometer, this should be a very effective elevation angle sensor for monitoring the approach and landing of aircraft. The interferometer-ambiguity revolving antenna complex for the terminal Air Traffic Control landing application is illustrated in Fig. 20.

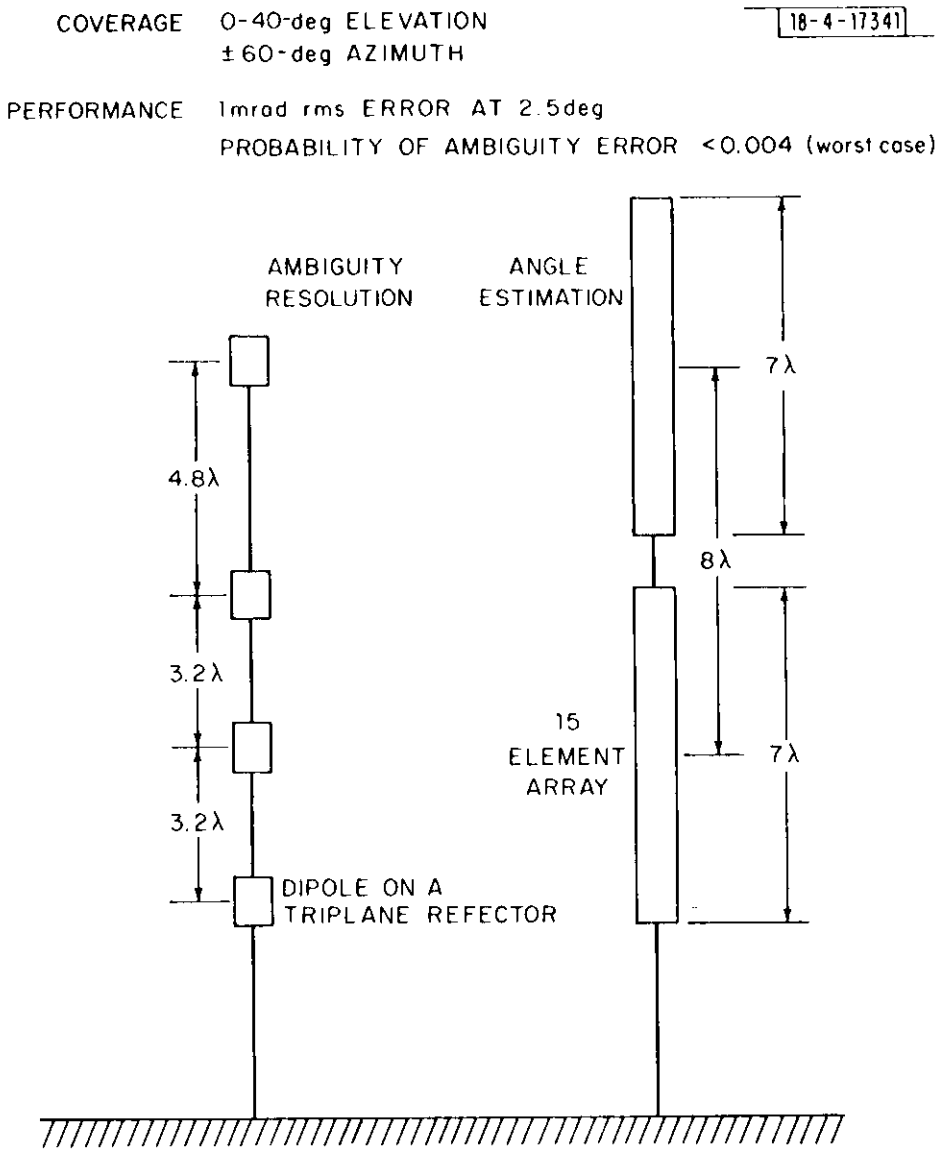

Fig. 20. Typical interferometer - ambiguity resolving antenna complex.

APPENDIX

Derivation of the Large SNR Error Probability

An upper bound on the conditional error probability was derived in equation (16). The result was the following:

$$P(\epsilon \mid e_s) \leq \sum_{\substack{k=0 \\ k \neq m}}^{M-1} P\left[\ell(k) > \ell(m) \mid \upsilon_s = \upsilon_0 + \frac{m}{T}\right] \quad . \tag{A. 1}$$

It was further shown that the likelihood ratios were given by

$$\ell(i) = \left|\gamma_s \lambda(\upsilon_s = \hat{\upsilon}_i) + \gamma_I \lambda(\upsilon_i - \hat{\upsilon}_i) + \eta(i)\right|^2 \tag{A. 2}$$

where $\eta(i)$ is a zero mean, complex Gaussian random variable with covariance

$$\overline{\eta(i)\,\eta^*(j)} = \frac{2\sigma^2}{N} \lambda(\hat{\upsilon}_i - \hat{\upsilon}_j) \tag{A. 3a}$$

$$\overline{\eta(i)\,\eta^*(j)} = 0 \quad . \tag{A. 3b}$$

The development is simplified somewhat by introducing the following additional notation:

$$\xi(i) = \gamma_s \lambda(\upsilon_s - \hat{\upsilon}_i) + \gamma_I \lambda(\upsilon_I - \hat{\upsilon}_i) \qquad i = k \text{ or } m \tag{A. 4}$$

Then

$$\begin{aligned} \ell(i) &= \left|\xi(i) + \eta(i)\right|^2 \\ &= \left|\xi(i)\right|^2 + 2\,\mathrm{Re}[\xi^*(i)\,\eta(i)] + \left|\eta(i)\right|^2 \\ &\approx \left|\xi(i)\right|^2 + 2\,\mathrm{Re}[\xi^*(i)\,\eta(i)] \end{aligned} \tag{A. 5}$$

where the last approximation holds when the effective signal-to-noise ratio is high (typically ~12 dB). The noise term becomes

$$z_i = 2\,\mathrm{Re}[\xi^*(i)\,\eta(i)] \tag{A.6}$$

which is a zero mean, real Gaussian random variable having variance

$$\overline{z_i^2} = \frac{4\sigma^2}{N}\,|\xi_i|^2 \quad . \tag{A.7}$$

The random variables z_m and z_k have covariance

$$z_m\,z_k = \frac{4\sigma^2}{N}\,\mathrm{Re}[\xi(m)\,\xi(k)\,\lambda\,(\hat{\upsilon}_m - \hat{\upsilon}_k)] \quad . \tag{A.8}$$

By definition, $\hat{\upsilon}_i = \hat{\upsilon}_0 + i/T$, hence equation (A.8) reduces to

$$z_m\,z_k = \frac{4\sigma^2}{N}\,\mathrm{Re}\left[\xi(m)\,\xi(k)\,\lambda\left(\frac{m-k}{T}\right)\right] \quad . \tag{A.9}$$

The purpose of the analysis is to find an expression for the conditional probability

$$P\left[\ell(k) > \ell(m) \,\middle|\, \upsilon_s = \upsilon_0 + \frac{m}{T}\right]$$

which can be used in equation (14). Using equations (A.5) and (A.6), the computation reduces to

$$P\left[\ell(k) > \ell(m) \,\middle|\, \upsilon_s = \upsilon_0 + \frac{m}{T}\right] = P\left[|\xi(k)|^2 + z_k > |\xi(m)|^2 + z_m \,\middle|\, \upsilon_s = \upsilon_0 + \frac{m}{T}\right]$$

$$= P\left[z_k - z_m > |\xi(m)|^2 - |\xi(k)|^2 \,\middle|\, \upsilon_s = \upsilon_0 + \frac{m}{T}\right] \quad . \tag{A.10}$$

However, z_k and z_m are zero mean Gaussian random variables; hence, $z_k - z_m$ is also a zero mean, Gaussian random variable. Furthermore, its variance is

$$\sigma_\Delta^2 = \overline{[z(k) - z(m)]^2}$$

$$= \frac{4\sigma^2}{N} \left\{ |\xi(k)|^2 + |\xi(m)|^2 - 2\,\mathrm{Re}\left[\xi(m)\,\xi^*(k)\,\lambda\left(\frac{m-k}{T}\right)\right]\right\} . \qquad \text{(A. 11)}$$

Therefore, it follows that

$$P\left[\ell(k) > \ell(m) \,|\, v_s = v_0 + \frac{m}{T}\right]$$

$$= \mathrm{erfc}\left(\frac{|\xi(m)|^2 - |\xi(k)|^2}{\sigma_\Delta}\right) \qquad \text{(A. 12)}$$

where

$$\mathrm{erfc}\,(x) = \frac{1}{\sqrt{2\pi}} \int_x^\infty \exp\left(\frac{-t^2}{d}\right)\, dt \qquad \text{(A. 13)}$$

denotes the error function.

The critical parameters in terms of system performance are usually the multipath reflection coefficient, $\rho = |\gamma_I|/|\gamma_s|$, and the relative phase between the direct and multipath signals, $\varphi = \arg \gamma_I - \arg \gamma_s$. These definitions are substituted into equation (A. 4), which can then be expressed as follows:

$$\xi(i) = \gamma_s[\lambda(v_s - \hat{v}_I) + \lambda(v_I - \hat{v}_I)\,\rho\, \exp \varphi] \quad . \qquad \text{(A. 14)}$$

Letting

$$\xi'(i) = \xi(i)/\gamma_s \tag{A. 15}$$

the argument of the error function becomes

$$\frac{|\xi(m)|^2 - |\xi(k)|^2}{\sigma_\Delta} =$$

$$\frac{1}{\sqrt{2}}\left(\frac{N|\alpha_s|^2}{2\sigma^2}\right) \frac{|\xi'(m)|^2 - |\xi'(k)|^2}{\left\{|\xi'(m)|^2 + |\xi'(k)|^2 - 2\,\mathrm{Re}\left[\xi'(m)\,\xi'(k)\,\lambda\left(\frac{m-k}{T}\right)\right]\right\}^{1/2}} \tag{A. 16}$$

Equations (A. 12) to (A. 16) are the bases for equations (26) to (30).

ACKNOWLEDGMENTS

The author would like to thank Dr. J. Evans for pointing out the details of the digital filter analog to the antenna design problem, and Dr. J. McClellan who supplied the computer algorithm for designing the optimum filters. The motivation and encouragement generated by Dr. J. Stiglitz were important to the initiation and completion of this work.

REFERENCES

[1] J.E. Evans, D. Karp, R.R. LaFrey, R.J. McAulay, and I.G. Stiglitz, "Experimental Validation of PALM - A System for Precise Aircraft Location," Technical Note 1975-29, Lincoln Laboratory, M.I.T. (29 April 1975), DDC AD-010112/1.

[2] R.N. Alcock, D.A. Lucas, and R.P. Vincent, "'MADGE,' A Microwave Aircraft Digital Guidance Equipment," Philips Technical Review 34, 225-241 (1974).

[3] M.I. Skolnik, Introduction to Radar Systems (McGraw-Hill, New York, 1962).

[4] J.W. Ducan, "The Effects of Ground Reflection on an Interferometer Direction Finder," IEEE Trans. Aerospace Electron, Systems AES-3, 922-932 (1967).

[5] J.L. Allen, "The Theory of Array Antennas (with Emphasis on Radar Applications)," Technical Report 323, Lincoln Laboratory, M.I.T. (25 July 1963), DDC AD-422945.

[6] J.E. Evans, "Synthesis of Equiripple Sector Antenna Patterns," IEEE Trans. Antennas Propag. (submitted for publication).

[7] T.W. Parks, and J.H. McClellan, "Chebyshev Approximation for Nonrecursive Digital Filters with Linear Phase," IEEE Trans. Circuit Theory, CT-19, 189-194 (1972).

[8] L.R. Rabiner and B. Gold, Theory and Application of Digital Signal Processing, Ch. 3 (Prentice Hall, New Jersey, 1975).

[9] E. Hofstetter, A.V. Oppenheim, and J. Siegal, "A New Technique for the Design of Nonrecursive Digital Filters," presented at 5th Annual Princeton Conf. Information Sciences and Systems, March 1971.

[10] R.N. Alcock, D.A. Lucas, and R.P. Vincent " "MADGE,' A Microwave Aircraft Digital Guidance Equipment," Philips Technical Review 34, 225-241 (1974).

[11] E.M. Hofstetter and D.F. Delong, "Detection and Parameter Estimation in an Amplitude-Comparison Monopulse Radar, "IEEE Trans. Inform. Theory IT-15, 22-30 (1969).

[12] H.L. Van Trees, Detection, Estimation, and Modulation Theory, Part I, Chapt. 2 (Wiley, New York, 1968).

[13] J.M. Wozencraft and I.M. Jacobs, Principles of Communication Engineering, Chapt. 4 (Wiley, New York, 1965).

[14] P. Bechman and A. Spizzichino, The Scattering of Electromagnetic Waves from Rough Surfaces (Macmillin, New York, 1963), p. 218.

[15] D. Kerr, Propagation of Short Radio Waves (Dover, New York, 1965).

[16] G. F. Spingler, "Experimentation and Analysis of Siting Criteria," FAA Report RD-69-43, FAA National Aviation Facilities Experimental Center, New Jersey (1969).

UNCLASSIFIED

SECURITY CLASSIFICATION OF THIS PAGE *(When Data Entered)*

REPORT DOCUMENTATION PAGE		READ INSTRUCTIONS BEFORE COMPLETING FORM
1. REPORT NUMBER ESD-TR-76-35	2. GOVT ACCESSION NO.	3. RECIPIENT'S CATALOG NUMBER
4. TITLE *(and Subtitle)* Optimum Elevation Angle Estimation in the Presence of Ground Reflection Multipath		5. TYPE OF REPORT & PERIOD COVERED Technical Note 6. PERFORMING ORG. REPORT NUMBER Technical Note 1976-11
7. AUTHOR*(s)* Robert J. McAulay		8. CONTRACT OR GRANT NUMBER*(s)* F19628-76-C-0002
9. PERFORMING ORGANIZATION NAME AND ADDRESS Lincoln Laboratory, M.I.T. P.O. Box 73 Lexington, MA 02173		10. PROGRAM ELEMENT, PROJECT, TASK AREA & WORK UNIT NUMBERS Program Element No. 65705F Project No. 649L
11. CONTROLLING OFFICE NAME AND ADDRESS Air Force Systems Command, USAF Andrews AFB Washington, DC 20331		12. REPORT DATE 9 February 1976 13. NUMBER OF PAGES 78
14. MONITORING AGENCY NAME & ADDRESS *(if different from Controlling Office)* Electronic Systems Division Hanscom AFB Bedford, MA 01731		15. SECURITY CLASS. *(of this report)* Unclassified 15a. DECLASSIFICATION DOWNGRADING SCHEDULE

16. DISTRIBUTION STATEMENT *(of this Report)*

Approved for public release; distribution unlimited.

17. DISTRIBUTION STATEMENT *(of the abstract entered in Block 20, if different from Report)*

18. SUPPLEMENTARY NOTES

None

19. KEY WORDS *(Continue on reverse side if necessary and identify by block number)*

elevation angle estimation
ground reflection multipath
terminal air traffic control
phase-comparison monopulse
interferometer
optimum antenna synthesis
finite impulse response
linear phase
digital filter

20. ABSTRACT *(Continue on reverse side if necessary and identify by block number)*

An optimal trade-off between the width of the subarray aperture and the width of the interferometer base line is performed that achieves a specified elevation angle estimation error while minimizing the overall height of the interferometer configuration. Statistical decision theory is used to analyze and design a separate sensor for resolving the interferometer ambiguities. For coverage over 2.5° to 40° in elevation and ±60° in azimuth, two 7-wavelength subarrays separated by 8 wavelengths are sufficient for 1-mrad elevation-angle errors. A 4-element nonuniformly spaced array of dipole antennas mounted on tri-plane reflectors renders the probability of an ambiguity error less than 0.004.

DD FORM 1 JAN 73 1473 EDITION OF 1 NOV 65 IS OBSOLETE

UNCLASSIFIED

SECURITY CLASSIFICATION OF THIS PAGE *(When Data Entered)*